The Meteoritical Society

Meteoritics & Planetary Science 45, Nr 12, 1982–2006 (2011)
doi: 10.1111/j.1945-5100.2010.01134.x

The Tucson ungrouped iron meteorite and its relationship to chondrites

G. KURAT[1,2†], M. E. VARELA[3*], E. ZINNER[4], and F. BRANDSTÄTTER[2]

[1]Department of Lithospheric Sciences, University of Vienna, Althanstrasse 14, 1090 Vienna, Austria
[2]Mineralogisch-Petrographische Abteilung, Naturhistorisches Museum, Burgring 7, 1010 Wien, Austria
[3]Instituto de Ciencias Astronómicas de la Tierra y del Espacio (ICATE), Av. España 1512 Sur, J5402DSP San Juan, Argentina
[4]Laboratory for Space Sciences and the Physics Department, Washington University, St. Louis, Missouri 63130, USA
[†]Deceased.
[*]Corresponding author. E-mail: evarela@icate-conicet.gob.ar

(Received 08 January 2010; revision accepted 24 August 2010)

Abstract–Tucson is an enigmatic ataxitic iron meteorite, an assemblage of reduced silicates embedded in Fe-Ni metal with dissolved Si and Cr. Both, silicates and metal, contain a record of formation at high temperature (~1800 K) and fast cooling. The latter resulted in the preservation of abundant glasses, Al-rich pyroxenes, brezinaite, and fine-grained metal. Our chemical and petrographic studies of all phases (minerals and glasses) indicate that they have a nebular rather than an igneous origin and give support to a chondritic connection as suggested by Prinz et al. (1987). All silicate phases in Tucson apparently grew from a liquid that had refractory trace elements at approximately 6–20 × CI abundances with nonfractionated (solar) pattern, except for Sc, which was depleted (~1 × CI). Metal seems to have precipitated before and throughout silicate aggregate formation, allowing preservation of all evolutionary steps of the silicates by separating them from the environment. In contrast to most chondrites, Tucson documents coprecipitation of metal and silicates from the solar nebula gas and precipitation of metal before silicates—in accordance with theoretical condensation calculations for high-pressure solar nebula gas. We suggest that Tucson is the most metal-rich and volatile-element-poor member of the CR chondrite clan.

INTRODUCTION

Tucson is a unique ataxitic iron meteorite with about 8 vol% silicates (mainly olivine) arranged in subparallel flow-like structures (Buchwald 1975). The high Si (0.8 wt%) and the very low Ge content of the metal (Wai and Wasson 1969) make Tucson distinctive among the iron meteorites with silicate inclusions (Wasson 1970). Silicate inclusions in Tucson, first reported by Smith (1855), have a remarkably reduced state (Cohen 1905), are depleted in volatile elements, and have on average approximately chondritic refractory lithophile element abundances (Wänke et al. 1983). The low iron content of the silicates, the high content of silicon in the metal, and the chalcophile behavior of vanadium, among other features, led Bunch and Fuchs (1969) to point out that Tucson shows similarities with enstatite chondrites and achondrites. Nehru et al. (1982) also explored the possible relationship between Tucson and the enstatite meteorites. On the other hand, Prinz et al. (1987) concluded that Tucson silicates have isotopic and chemical similarities with constituents from carbonaceous chondrites such as Bencubbin, Kakangari, and Renazzo.

Here, we report the result of a compositional (major and trace element) study of the phases constituting the silicate inclusions of this meteorite. We examined their petrological relationships with each other and with other meteoritic rocks and discuss the possible ways in which Tucson silicates could have formed. Preliminary results were presented at the Lunar and Planetary Science Conference in Houston, Texas, and the Meteoritical Society Meeting in Nancy, France (Varela et al. 2008, 2009, 2010).

ANALYTICAL TECHNIQUES AND SAMPLES

Silicate inclusions were studied in the thin section L3951 and the thick polished section Tucson B (NHM,

Vienna). The nonmetallic phases in the Tucson iron were studied with an optical microscope and a scanning electron microscope. Major element chemical compositions were obtained with a JEOL 6400 analytical scanning electron microscope and ARL-SEMQ and CAMECA SX100 electron microprobes (EMP) (NHM, Vienna; Department of Lithospheric Science, University of Vienna; and ICATE, San Juan, Argentina). Microprobe analyses were performed at 15 kV (silicates) and 20 kV (metal and sulfide) acceleration potential and 15 nA sample current. Trace element analyses of silicates and sulfides were made with the Cameca IMS 3F ion microprobes at Washington University (St. Louis) and Max-Planck-Institut für Chemie (Mainz), following a modified procedure of Zinner and Crozaz (1986).

RESULTS

Petrography of Silicate Inclusions and Sulfides

The ungrouped iron Tucson contains about 8 vol% silicate inclusions (Buchwald 1975), which are arranged in a way that is reminiscent of flow structures (Bunch and Fuchs 1969; Miyake and Goldstein 1974; Buchwald 1975). They cover metal nodules and are arranged along huge bent plates (Figs. 1a and 1b). Round aggregation structures of metal nodules and silicate inclusion are dominant in the cut surface of sample A 726 (Fig. 1a) from the Naturhistorisches Museum in Vienna, and are also abundant in other samples, e.g., the Smithsonian Institution's sample U.S.N.M. no. 757 (see fig. 1801 in Buchwald 1975, p. 1237).

Silicate inclusions range in size from < 10 μm to about 1200 μm in sections L3951 and Tucson B (Figs. 2a–h). Inclusions of different shape and size occur in different plate aggregates. Large inclusions are elongated and are oriented parallel to the "flow" structure. There is also some correlation with inclusion size and the number of different phases present. *Small silicate inclusions* (∼40–∼100 μm)—which generally have round and smooth interfaces toward metal—are mostly composed of one (olivine) or two phases (olivine and glass; Figs. 2a–d). The single olivine inclusion in Fig. 2b has an inclusion which consists of glass, a metal globule, and a bubble. The two-phase silicate inclusions have mesostasis glass between olivines or surrounding the olivine (Figs. 2c and 2d). The olivine has crystal faces against glass but round interfaces with metal—as has previously been described by Nehru et al. (1982). Perfectly spherical glass-rich objects are rare and contain a single euhedral olivine with crystal faces against the glassy mesostasis (Fig. 2d). Other small inclusions consist of an olivine crystal which is completely covered by Ca-poor, Al-rich orthopyroxene and small amounts of aluminous Ca-rich pyroxene (Figs. 3a and 3b). Very common are also small inclusions made mainly of a single olivine crystal that is partly covered by Ca-poor, Al-rich orthopyroxene which forms intergrowths with brezinaite (symplectitic) and kamacite (inclusions; Figs. 3c and 3d).

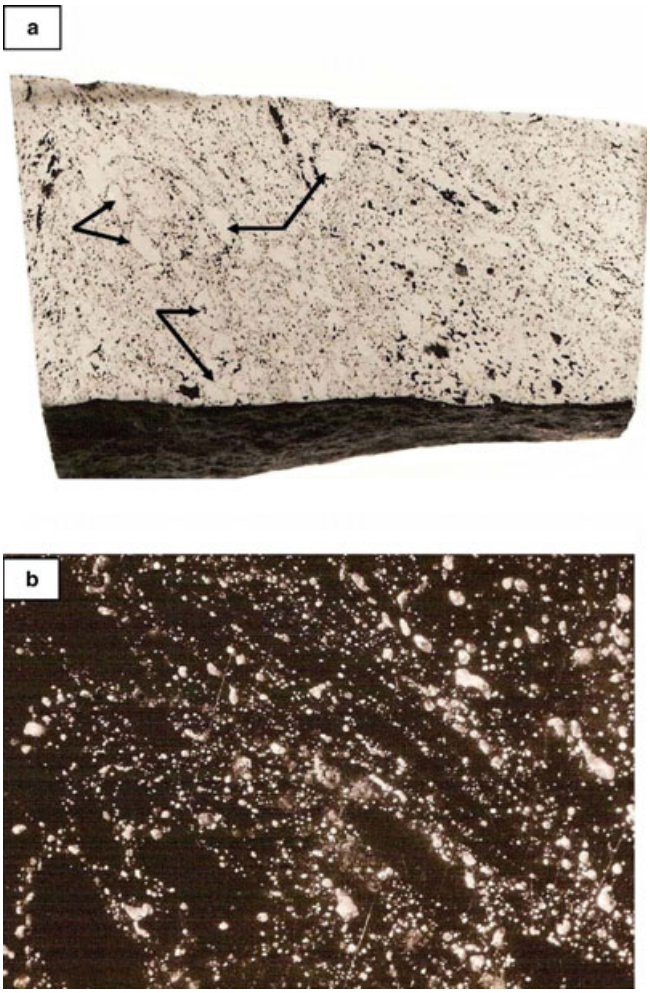

Fig. 1. a) Polished surface of Tucson sample inventory no. A 726 (Naturhistorisches Museum, Vienna, 396 g) showing "flow" and aggregation structures. Centimeter-sized aggregates consist of metal nodules (arrows) decorated by silicates. Between the aggregates are situated elongated metal nodules and sheets of silicate aggregates (details in b). Length of sample is approximately 8 cm. b) Dark field optical picture (the sample is illuminated with light that is not collected by the objective lens) of the polished surface of sample M 8617 (Naturhistorisches Museum, Vienna) of the Tucson iron showing the arrangement of silicate inclusions (gray) around metal (black) nodules (left) and along planes. Note the range of sizes of silicate inclusions: small ones dominate the central streaky arrays and surfaces of metal nodules (left side), and large ones dominate the right upper region. Sample length is approximately 4 cm.

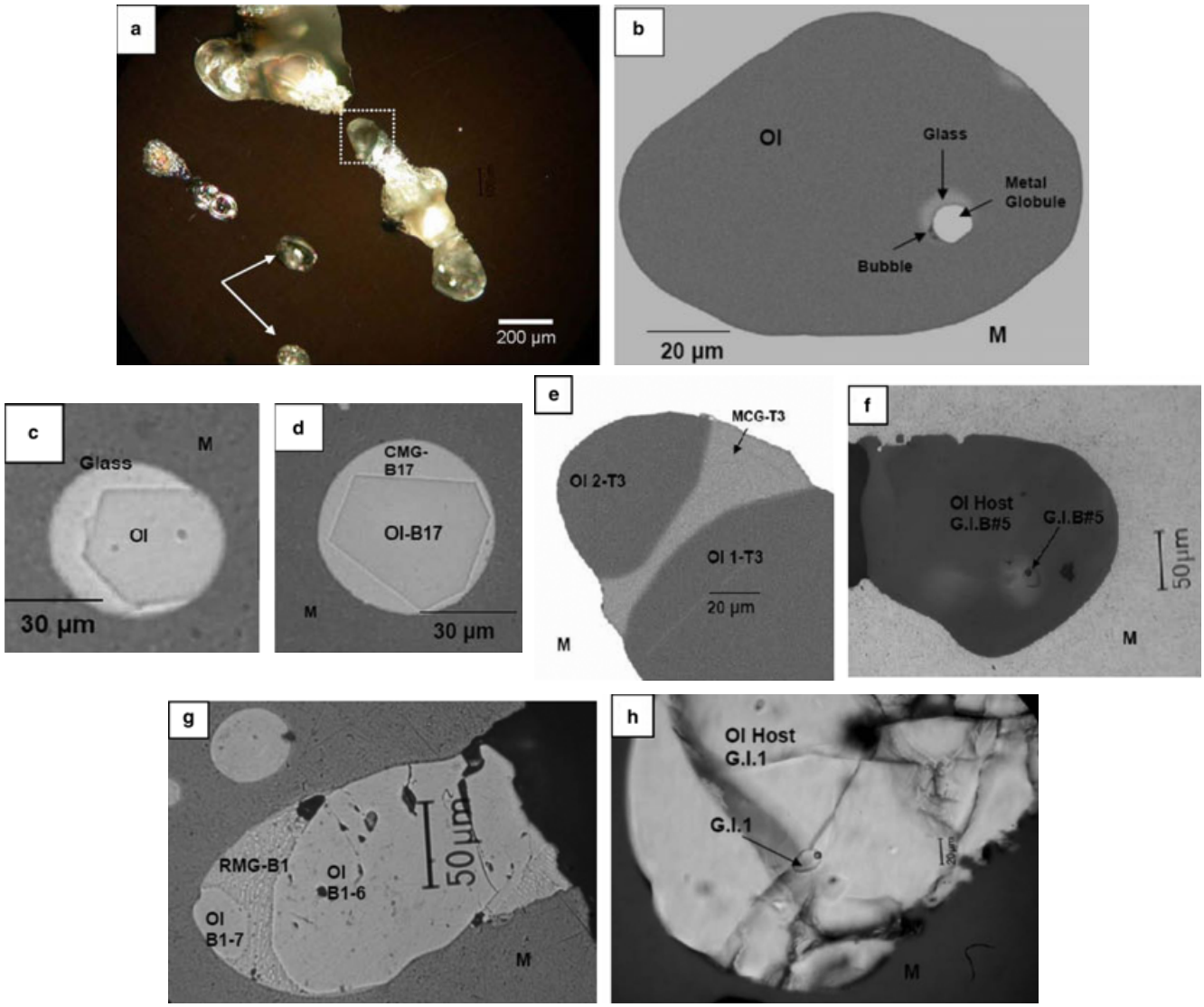

Fig. 2. a) Three large olivine-rich silicate inclusions (center, left, and upper left) and two-phase (olivine + glass) small ones (arrows). Inclusions are elongated in the direction of the general ''flow'' pattern. Optical image, crossed polarizers. b) BSE image of a small single olivine with an inclusion consisting of a metal globule, glass, and a bubble. c) Reflected light image of a small silicate inclusion in metal (M, gray), consisting of an olivine (Ol, light gray) and glass (white). Note the olivine crystal faces in contact with glass and the round interface in contact with metal. d) Reflected light image of a small silicate inclusion in metal (M, gray) consisting of an olivine crystal (Ol-B17, light gray) and glass (CMG-B17). Note the perfectly round shape of the inclusion and the perfectly developed crystal faces of the olivine. e) BSE image of upper end of central inclusion in (a) (stippled square) with clear mesostasis glass (CMG-T3) between olivines (Ol 2-T3 and Ol 1-T3). f) Olivine (Ol Host G.I.B#5) and glass inclusion G.I.B#5 with bubble; from lower end of central silicate inclusion in (a). Reflected light image. g) Reflected light image of olivines Ol B1-6 and Ol B1-7 with recrystallized mesostasis glass (RMG-B1) from a large silicate inclusion. Note small glass-rich silicate inclusion at upper left. h) Reflected light image (partly crossed polarizers) of glass inclusion G.I.1 with bubble in olivine (Ol Host G.I.1) of a large silicate inclusion.

Large silicate inclusions are elongated multiphase rocks with serrated and/or smooth surfaces against metal. They consist of olivine and pyroxenes—as major phases—with minor glass or crystalline mesostasis, metal, and brezinaite (Figs. 4a and 4b). Olivine in these inclusions is always poikilitically included in or partly covered by Ca-poor, Al-rich orthopyroxene. The orthopyroxene also commonly forms symplectites with brezinaite and carries metal inclusions (Fig. 4c)—as in small inclusions. Very large inclusions (Fig. 4b) frequently consist of rounded olivines and angular clino-enstatites (Ca-poor and Al-poor), which are poikilitically enclosed by Ca-poor, Al-rich orthopyroxene. Poikilitic pyroxene has smooth interfaces with olivine, other

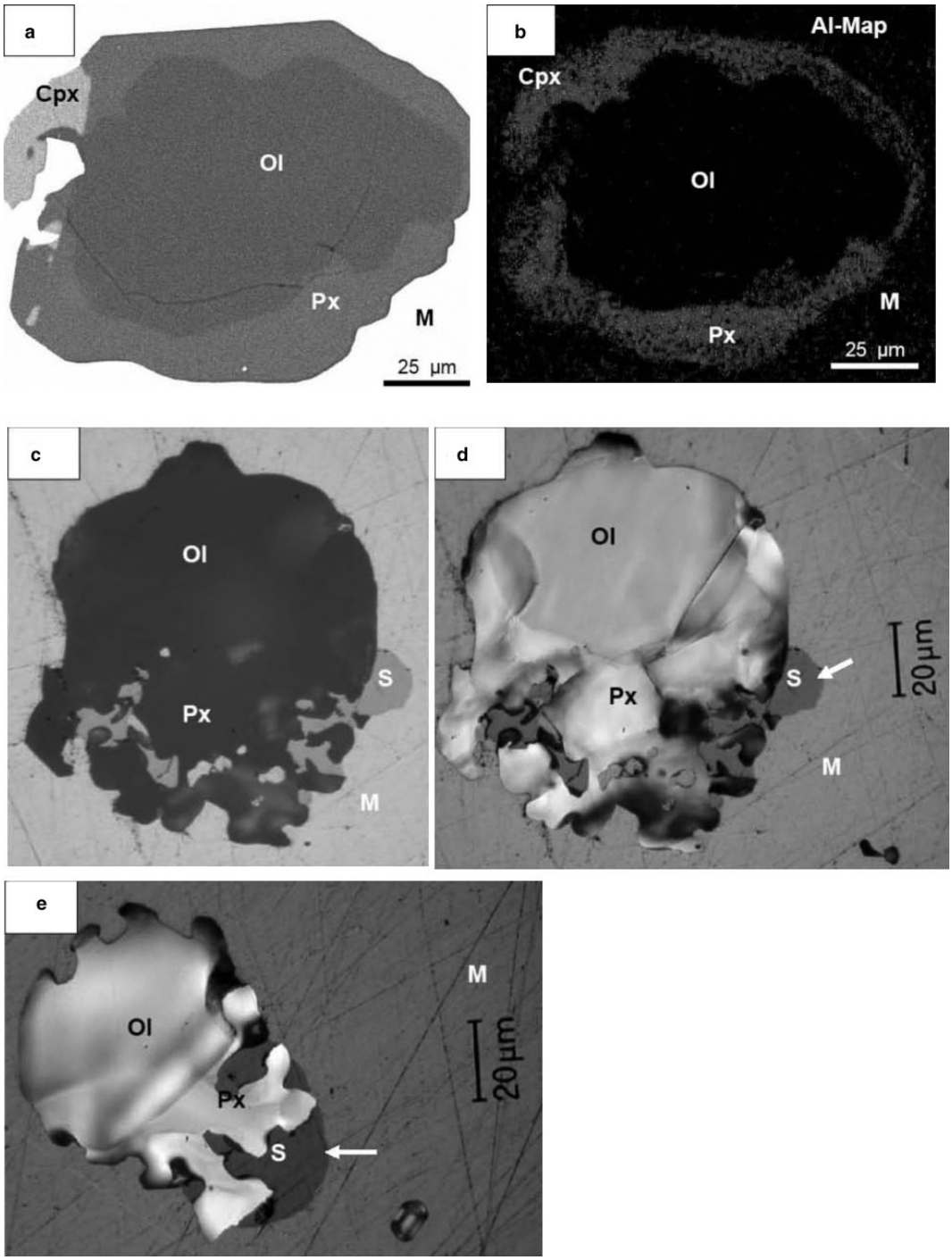

Fig. 3. a) BSE image of olivine single crystal (Ol) covered by Al-rich low-Ca pyroxene (Px) and Ca-rich clinopyroxene (Cpx) in metal (M). b) Map of Al distribution of area shown in (a). Note the highly variable Al content of the Ca-poor pyroxene. c) Optical image of a small silicate inclusion consisting of an olivine (Ol) and low-Ca pyroxene (Px)—brezinaite (S) symplectite. Note the well-developed brezinaite meniscus at the right surface of the inclusion (white arrow) and the rounded surfaces of all silicates against metal (M). d) Same object, image with partly crossed polarizers. e) Optical image (partly crossed polarizers) of small silicate inclusion consisting of olivine (Ol) and low-Ca pyroxene (Px)—brezinaite (S) symplectite in metal. Note the meniscus (white arrow) formed by brezinaite against metal (M) and the very small olivine-glass inclusion in metal at lower right.

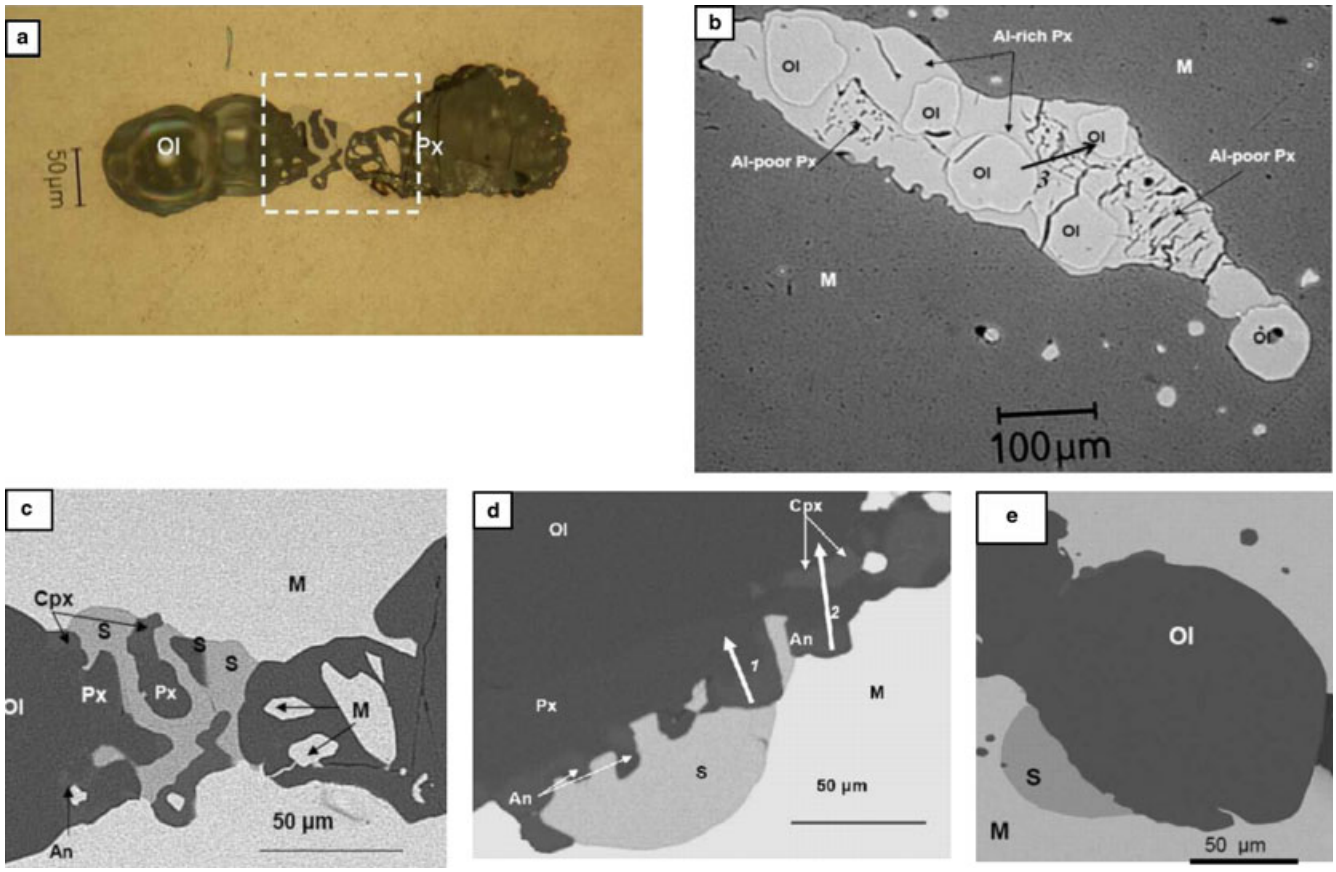

Fig. 4. a) Reflected light image of a multiphase silicate inclusion (enlargement from Fig. 2a, left) consisting of low-Ca pyroxene (right) and olivine (±glass, left), which are connected by symplectitic intergrowth of Al-rich pyroxene and brezinaite (left) and a complex intergrowth of Al-rich pyroxene and metal (right) (see details in c). The olivine-rich part has a smooth interface toward the metal but pyroxene has a complex one. b) Reflected light image of a large silicate inclusion consisting of rounded olivines and angular clino-enstatite (cracked) embedded in Al-rich orthopyroxene (smooth surface). The interface of Al-rich pyroxene toward metal is mostly smooth but also rugged in places. There is no glass or crystalline mesostasis exposed on this inclusion (see Profile 3, Table 1). c) BSE image of center portion of silicate inclusion shown in (a) (stippled square). Low-Ca, Al-rich pyroxene (Px), Ca-rich pyroxene (Cpx) and anorthite (An) forms symplectitic intergrowths with brezinaite (S, light gray) on the left and with kamacite on the right. Note the crystal faces shown by kamacite (M) enclosed in Al-rich orthopyroxene. The metal included in pyroxene has the shape of prismatic pyroxene crystals. d) BSE image of brezinaite (S) forming a meniscus toward the metal (M, white) and a symplectitic intergrowth with low-Ca pyroxene (Px), Ca-rich pyroxene (Cpx) and anorthite (An)—all on top of an olivine (Ol) of a large silicate inclusion (see Profiles 1 and 2, Table1). e) BSE image of olivine (Ol) from large silicate inclusion with brezinaite (S) meniscus toward metal (M).

pyroxenes, and anorthite. It has either smooth or serrated interfaces with metal and forms symplectitic intergrowths with brezinaite (Figs. 4a–c). Anorthite and Ca-rich, Al-rich pyroxene are scarce and the tiny grains are generally associated with Ca-poor, Al-rich orthopyroxene in contact with brezinaite (Figs. 4c and 4d).

Brezinaite is the only sulfide present in Tucson (Buchwald 1975). It is always associated with pyroxenes and commonly forms symplectitic intergrowths with pyroxenes (±anorthite, Al-diopside) (Figs. 3c–e, 4c, and 4d). In contrast to the complex interfaces toward pyroxenes, brezinaite commonly has smooth menisci toward metal (Figs. 4d and 4e) and also smooth interfaces toward olivine (Fig. 3d).

Glasses and mesostasis: Olivine in small and large silicate inclusions occasionally contains primary glass-bearing inclusions. These inclusions have sizes varying between 5 and 35 µm, rounded or subrounded shapes and are found in clusters (Figs. 2f and 2h) and as isolated inclusions (Fig. 2b). Most of them consist of clear glass and a shrinkage bubble. A few are multiphase inclusions that contain glass, metal, and a shrinkage bubble (Fig. 2b). All glasses of glass-bearing inclusions are clear without signs of devitrification.

Mesostasis mainly is present between olivines or is enveloping olivine in small inclusions (Figs. 2e and 2g). It can either consist of clear glass (e.g., CMG [clear

Table 1. Major element composition of silicates in Tucson (in wt%).

	Coexisting phases												
	Profile 1				Profile 2				Profile 3				
	An	Al-Px	Al-Px	Ol	An	Al-Px	Cpx	Ol	Ol	Al-Px	Px	Al-Px	Ol
SiO_2	42.7	49.1	48.7	42.6	42.7	48.5	50.7	42.5	41.9	54.6	57.8	52.7	41.9
TiO_2	bdl	0.11	0.14	bdl	bdl	0.20	0.22	bdl	bdl	0.32	0.06	0.04	bdl
Al_2O_3	36.1	17.0	12.9	0.07	34.9	17.7	7.3	0.07	0.04	6.3	0.6	9.2	0.04
Cr_2O_3	bdl	0.11	0.09	bdl	0.08	0.10	0.06	bdl	bdl	0.11	0.07	0.11	bdl
FeO	0.6	0.37	0.28	0.28	0.8	0.49	0.46	0.38	0.27	0.27	0.25	1.1	0.32
MnO	bdl	bdl	bdl	bdl	bdl	bdl	bdl	bdl	bdl	bdl	bdl	bdl	bdl
MgO	0.9	31.9	38.5	56.6	1.2	31.7	17.7	56.3	57.6	36.1	39.0	34.4	57.4
CaO	19.3	1.3	0.9	0.10	19.7	1.2	23.1	0.10	0.12	1.1	0.42	0.36	0.10
Na_2O	bdl	bdl	bdl	bdl	0.03	bdl	bdl	bdl	bdl	bdl	bdl	bdl	bdl
K_2O	bdl	bdl	bdl	bdl	bdl	bdl	bdl	bdl	bdl	bdl	0.03	0.03	bdl
Total	99.6	99.9	101.4	99.7	99.4	99.9	99.6	99.3	99.9	98.8	98.2	97.9	99.8

	Coexisting pyroxenes					
	Px2-B8 = 0.84* (6)	Px1-B8 = 3.15* (6)	Cpx B4* (2)	Px-B4 = 9.43* (3)	Px-B3 = 0.7* (3)	Px-B3 = 9.8* (2)
SiO_2	59.3	57.5	49.3	53.5	59.2	52.8
TiO_2	0.06	0.12	0.6	0.29	bdl	0.33
Al_2O_3	0.84	3.15	9.8	9.43	0.70	9.8
Cr_2O_3	bdl	bdl	bdl	bdl	bdl	bdl
FeO	0.27	0.29	0.8	0.7	0.46	0.6
MnO	bdl	bdl	bdl	bdl	bdl	bdl
MgO	39.0	37.6	17.2	34.8	38.6	34.3
CaO	0.44	1.3	22.6	1.5	0.35	1.9
Na_2O	bdl	bdl	bdl	bdl	bdl	bdl
K_2O	bdl	bdl	bdl	bdl	bdl	bdl
Total	99.9	100.0	100.3	100.2	99.3	99.7

Note: Profile 1 (white arrow in Fig. 4d); Profile 2 (white arrow in Fig. 4d); Profile 3 (black arrow in Fig 4b); bdl = below detection limit; Px2-B8 = 0.84: low-Ca pyroxene (0.84 wt% Al_2O_3); (6) = mean of six analyses; detection limits (in ppm): TiO_2 (320); Cr_2O_3 (440); MnO (300); Na_2O (280); K_2O (280).

*Phases with secondary ion mass spectrometry analysis.

mesostasis glass]; Fig. 2e) or recrystallized glass (e.g., RMG [recrystallized mesostasis glass]; Fig. 2g). Olivine has crystal faces in contact with both mesostasis glasses (Figs. 2c–e and 2g).

Major Element Phase Compositions

Representative and averaged EMP analyses of the phases encountered in this study are given in Tables 1–2.

All silicate phases are poor in Fe, Mn, Cr, and alkali elements. Olivine typically has FeO contents between 0.19 and 1.38 wt% with most of the analyses clustering near the lower end of the range. The Al_2O_3 content is slightly variable (< 0.03–0.11 wt%) with CaO contents varying from 0.08 to 0.19 wt%. The contents of MnO and TiO_2 are below the detection limit of the EMP (330 and 320 ppm, respectively).

Pyroxenes have highly varying chemical compositions. The cracked, polysynthetically twinned clinoenstatite, which is commonly associated with olivine in large multiphase aggregates, has Al_2O_3 and CaO contents of 0.66–1.83 and 0.35–0.51 wt%, respectively. The FeO content varies from 0.25 to 0.46 wt% and the TiO_2 and Cr_2O_3 contents from 0.04 to 0.08 wt% and < 0.04 to 0.07 wt%, respectively. The contents of Mn, Na, and K are mostly below the detection limit of the EMP.

Aluminum-rich, Ca-poor orthopyroxene, which poikilitically encloses olivine and Al-poor clinoenstatite, has Al_2O_3 contents between approximately 2 and 18 wt%. It is poor in FeO (0.5–0.8 wt%) and Cr_2O_3 (0.04–0.08 wt%), contains some TiO_2 (up to 0.4 wt%) but is free of Mn and alkali elements.

Calcium-rich clinopyroxenes are present as small grains in contact with anorthite and Al-rich orthopyroxene that form serrated surfaces and symplectitic intergrowths with brezinaite. Clinopyroxene also has highly variable Al_2O_3 contents, which vary from about 7 to 17.7 wt%. It is also poor in FeO (~0.4–0.7 wt%), contains some TiO_2 (0.1–0.2 wt%) and Cr_2O_3 (up to 0.06 wt%), but no significant amounts of Mn and alkali elements.

Table 2. Major element composition of glasses (glass inclusions and mesostasis) and olivine (in wt%).

	Mesostasis and coexisting olivines													
	S. I. T3			S. I. T4			S. I. B16			S. I. B17		S. I. B1		
	CMG-T3 (5)*	Ol 2-T3	Ol 1-T3*	CMG-T4 (2)*	Ol22-T4	Ol23-T4	CMG-B16 (4)	Ol47-B16	Ol49-B16	CMG B17 (2)	OlB-17	RMG-B1 (33)*	OlB1-6	OlB1-7
SiO_2	49.2	42.0	42.1	48.9	42.2	42.2	49.7	42.6	42.2	48.4	42.6	49.2	41.1	42.2
TiO_2	bdl	bdl	bdl	bdl	bdl	bdl	bdl	bdl	bdl	bdl	bdl	0.05	bdl	bdl
Al_2O_3	28.1	bdl	bdl	28.3	bdl	bdl	27.7	0.08	0.06	29.8	bdl	25.9	0.06	0.11
Cr_2O_3	bdl	bdl	bdl	bdl	bdl	bdl	bdl	bdl	bdl	bdl	bdl	0.09	bdl	0.05
FeO	0.44	0.23	0.42	0.8	0.7	0.8	0.9	0.49	0.48	0.34	0.41	0.7	0.31	0.45
MnO	bdl	bdl	bdl	bdl	bdl	bdl	0.01	bdl	bdl	bdl	bdl	bdl	bdl	bdl
MgO	2.7	56.7	56.9	3.6	56.9	56.8	2.6	56.7	56.8	3.95	56.7	6.6	57.6	56.2
CaO	20.1	0.11	0.12	19.8	0.08	0.08	18.5	0.12	0.13	17.5	0.11	17.4	0.12	0.10
Na_2O	bdl	bdl	bdl	bdl	bdl	bdl	bdl	bdl	bdl	bdl	bdl	bdl	bdl	bdl
K_2O	0.03	bdl	bdl	bdl	bdl	bdl	bdl	bdl	bdl	bdl	bdl	bdl	bdl	bdl
Total	100.5	99.0	99.5	101.3	99.9	99.9	99.4	100.0	99.7	100.0	99.8	100.0	99.2	99.1

	Glass inclusions and host olivines									
	S. I. T1		S. I. T6		S. I. B#5		S. I. B5		S. I. B16	
	G.I.1*	Ol Host*	G.I.T6	Host Ol (15)	G.I.B#5*	Ol Host*	G.I.B5 (3)	Host Ol	G.I. B16	Host Ol
SiO_2	57.0	42.8	56.6	42.3	56.8	42.4	56.6	42.5	53.9	42.6
TiO_2	bdl	bdl	bdl	bdl	bdl	bdl	bdl	bdl	bdl	bdl
Al_2O_3	21.4	bdl	21.1	bdl	21.3	bdl	22.0	0.09	24.9	bdl
Cr_2O_3	bdl	bdl	bdl	bdl	bdl	bdl	bdl	bdl	bdl	bdl
FeO	0.19	0.19	0.35	0.49	0.27	0.3	1.3	1.4	0.6	0.49
MnO	bdl	bdl	bdl	bdl	bdl	bdl	bdl	bdl	bdl	bdl
MgO	1.6	57.2	3.3	57.4	2.5	56.4	2.1	56.5	1.7	56.7
CaO	19.6	0.16	18.9	0.10	19.2	0.12	18.3	0.19	17.6	0.10
Na_2O	bdl	bdl	bdl	bdl	bdl	bdl	0.06	bdl	0.03	bdl
K_2O	bdl	bdl	bdl	bdl	bdl	bdl	bdl	bdl	bdl	bdl
Total	99.8	100.4	100.3	100.3	100.1	99.2	100.4	100.7	98.7	99.9

Note: S.I. = silicate inclusion; CMG = clear mesostasis glass; MRG = recrystallized mesostasis glass; (33) = mean of 33 analyses; G.I. = glass inclusion; bdl = below detection limit; detection limits (in ppm): TiO_2 (320); Al_2O_3 (150); Cr_2O_3 (440); MnO (300); Na_2O (280); K_2O (280).

*Phase with secondary ion mass spectrometry analysis.

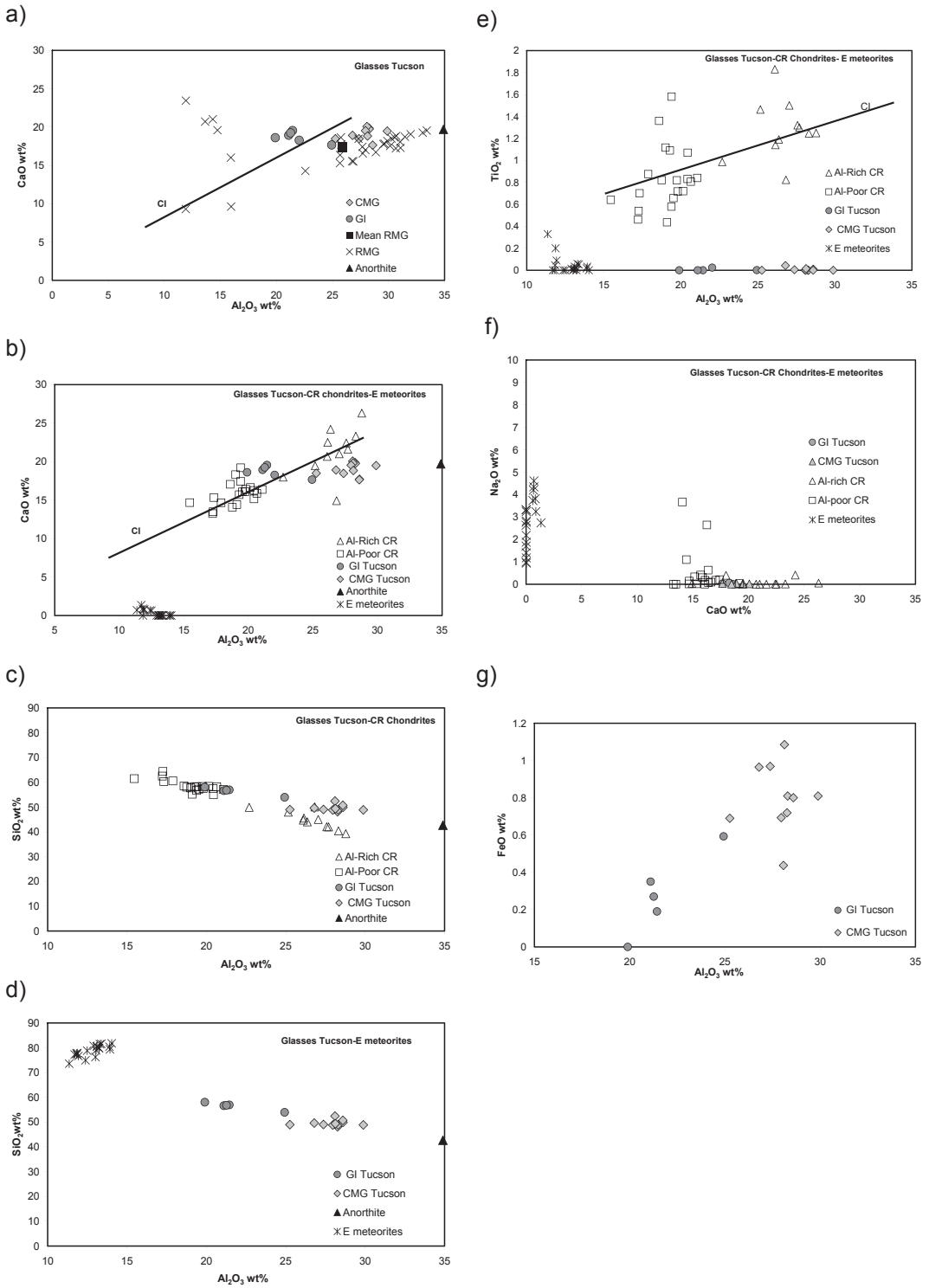

Fig. 5. Variation plots for major element contents (wt%) in glasses and matrices of Tucson silicate inclusions compared to glasses from enstatite meteorites (E meteorites) and CR chondrites. a) CaO versus Al_2O_3: individual analyses and average of recrystallized glasses with CI ratio reference line and anorthite projection point. b) CaO versus Al_2O_3: Tucson clear glasses compared to CR and E meteorite clear glasses with CI ratio reference line and anorthite projection point. c) SiO_2 versus Al_2O_3: Tucson and CR chondrite glasses and anorthite projection point. d) SiO_2 versus Al_2O_3: Tucson glasses, E meteorite glasses, and anorthite projection point. e) TiO_2 versus Al_2O_3: Tucson, CR chondrite, and E meteorite glasses with CI ratio reference line. Note that the TiO_2 content in Tucson glasses matched those in E meteorites. f) Na_2O versus CaO: Tucson, CR chondrite, and E meteorite glasses. g) FeO versus Al_2O_3: Tucson glass from glass inclusions in olivine and mesostasis.

Glasses (e.g., primary glass inclusions in olivine and mesostasis glass) have a Ca-Al-Si-rich composition (Table 2). Inclusion glass (GI) and CMG have similar CaO contents (~20 wt%; Figs. 5a and 5b) but differ in their Al_2O_3 and SiO_2 contents. GIs have Al_2O_3 and SiO_2 contents varying from 21 to 24.9 wt% and from 53.9 to 57 wt%, respectively. Concentrations in the mesostasis glass vary from 25.9 to 28.3 wt% Al_2O_3 and 48.1–49.2 wt% SiO_2. This results in a superchondritic CaO/Al_2O_3 ratio for GI and a subchondritic one for the CMG (Figs. 5a and 5b). GIs as well as mesostasis glasses are very poor in TiO_2 and FeO, which vary from <0.03 to 0.6 wt% and 0.5–1.18 wt%, respectively. Both types of clear glasses are also very poor in Cr_2O_3, MnO, and alkali elements (all <0.03 wt%).

Recrystallized mesostasis glass (Table 2) is highly variable in its Al_2O_3 content with the mean value (mean RMG; Fig. 5a) close to that of CMGs, which have a subchondritic CaO/Al_2O_3 ratio.

Metal is chemically homogeneous and there is no detectable significant chemical variation between the host metal (Si: 0.87 wt%, Ni: 9.4 wt%), the metal inside silicate inclusions (Si: 0.88 wt%, Ni: 9.5 wt%; Figs. 4a and 4c) and the metal globule inside a glass-bearing inclusion in olivine (Si: 0.74 wt%, Ni: 9.1 wt%; Fig. 2b).

Brezinaite (Cr_3S_4) contains minor amounts of Fe (0.7–3.2 wt%; Fig. 6), Mn (0.5–1.4 wt%), V (1.5–1.8 wt%), and Ti (0.5–1.2 wt%).

Trace Elements in Silicate Phases and Brezinaite

Glasses of glassy inclusions in olivine (Table 3) have high refractory element contents with abundances around $10 \times$ CI (Fig. 6a). Exceptions are Nb ($\sim 0.1 \times$ CI), Ti ($\sim 0.1 \times$ CI), Sc ($\sim 1 \times$ CI), and V ($\sim 0.5 \times$ CI), which are depleted with respect to the other refractory trace elements. The rare earth elements (REE) in glass inclusions in olivine have unfractionated to very slightly fractionated ($La_N > Lu_N$) patterns with abundances varying around $5–10 \times$ CI. Moderately, volatile element Li is depleted in G.I.B.#5 ($\sim 3 \times$ CI) but not in G.I.1 and Cr and Mn are strongly depleted with respect to the refractory elements.

Clear mesostasis glasses CMG-T3 and CMG-B17 as well as recrystallized matrix glass RMG-B1 have trace element abundances very similar to those of GIs (Fig. 6b). The refractory elements have abundances between about $5 \times$ CI and $20 \times$ CI. Exceptions are again Nb ($\sim 0.1 \times$ CI), Ti ($\sim 0.1 \times$ CI), Sc ($\sim 1 \times$ CI), and V ($\sim 0.1 \times$ CI), which are depleted with respect to the other refractory elements. The moderately volatile element Li has in all samples a higher normalized abundance than the refractory elements ($\sim 10 \times$ CI) and Cr and Mn are strongly depleted ($\sim 0.04 \times$ CI). The CMG-T3 is richer in most refractory trace elements than all other glasses (up to $\sim 75 \times$ CI for Ba; Fig. 6b) and it has a fractionated REE pattern with $La_N > Lu_N$ and abundances between 7 and $30 \times$ CI. It also has high contents of Zr ($\sim 20 \times$ CI), Y ($\sim 10 \times$ CI), Sr ($\sim 30 \times$ CI), Li ($\sim 25 \times$ CI), and Ba ($\sim 75 \times$ CI). The moderately volatile elements Cr and Mn are depleted similar to the refractory elements Ti and Nb with respect to all other refractory lithophile elements ($\sim 0.05 \times$ CI; Figs. 6a and 6b).

Volatile alkali elements such as Na and K have variable and very low abundances in all glasses (Table 3). Moderately volatile Li is present in all glasses at the abundance level of the refractory lithophile elements ($10–20 \times$ CI), except for inclusion glass G.I.B.#5, which is clearly poorer in Li ($\sim 3 \times$ CI) than all other glasses.

Olivines are very poor in trace elements and their abundances vary over wide ranges (Fig. 6c; Tables 3 and 4). The REE have low abundances ranging from $< 0.01 \times$ CI (LREE) to approximately $0.1–0.2 \times$ CI (Lu). Other incompatible elements have also low abundances, notably Zr, Sr, Nb, and Ba ($< 0.01 \times$ CI) and Y ($0.01–0.06 \times$ CI). Abundances of Ti, Ca, V, and Cr are between approximately 0.1 and $0.2 \times$ CI and Sc and Li between approximately 0.2 and $1 \times$ CI). The Mn content is very low at approximately $0.02 \times$ CI.

Trace element abundances in Al-poor, Ca-poor clinopyroxenes (Table 4; Px-B3 = 0.7 and Px2-B8 = 0.84 in Fig. 6d) are low: Nb and Sr at $\sim 0.01 \times$ CI, Zr, Y, MREE, Ba and Mn at $\sim 0.05 \times$ CI, Ca, LREE, HREE, V and Cr at $\sim 0.1 \times$ CI, and Ti, Sc and Li at $\sim 1 \times$ CI. The relatively high contents of LREE in Px2-B8 = 0.84 probably originate from terrestrial contamination.

Aluminum-rich orthopyroxenes are rich in trace elements with abundances about one order of magnitude higher than in low-Al pyroxenes (Table 4; Px-B3 = 9.8, Px-B4 = 9.43, and Px1-B8 = 3.15 in Fig. 6d): Sr at $\sim 0.02 \times$ CI (except Px-B4 = 9.43 with $\sim 0.2 \times$ CI), Nb at ~0.02 (Px1-B8A = 3.15) and $0.2 \times$ CI, Ba and Mn at $\sim 0.05 \times$ CI, LREE at $\sim 0.1 \times$ CI, V and Cr at $0.1–0.9 \times$ CI, Zr, Y, Ca at $\sim 0.8 \times$ CI, Sc, HREE and Li at $\sim 1 \times$ CI, and Ti at $\sim 3 \times$ CI.

Calcium-rich clinopyroxene (Table 4, Cpx B4 in Fig. 6d) has high trace element contents and an almost flat REE abundance pattern with roughly solar relative abundances, except for deficits in Sc, and Ti. It has low contents of Nb ($\sim 2 \times$ CI), Ba ($\sim 1.5 \times$ CI), V and Cr ($0.1–0.7 \times$ CI), and Mn ($\sim 0.07 \times$ CI).

Anorthite (Table 4; Fig. 6e) has a strongly fractionated trace element abundance pattern with high contents of Sr, Ba, and Eu ($\sim 10 \times$ CI), low contents of

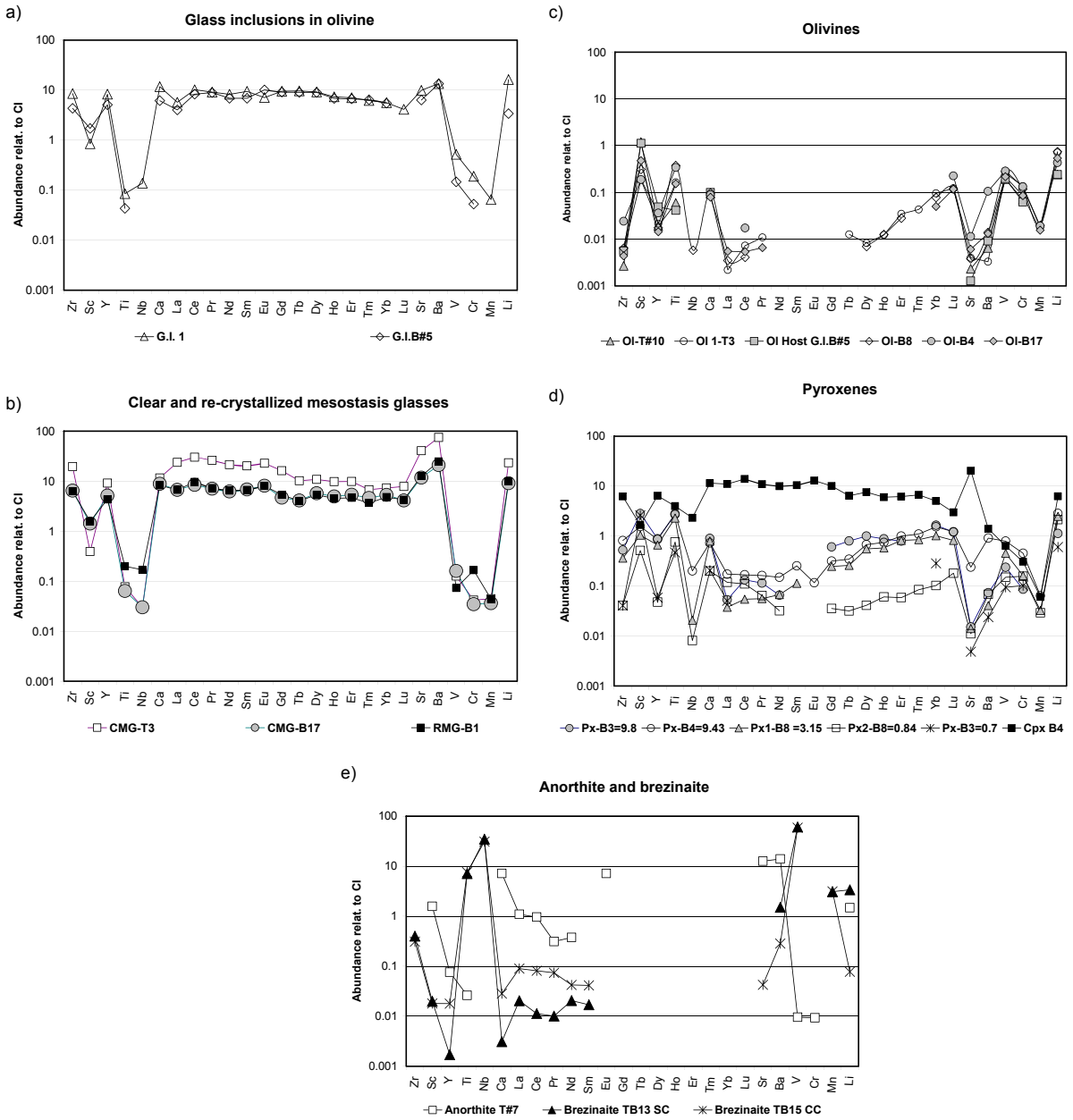

Fig. 6. CI-normalized (Lodders and Fegley 1998) trace element abundances in silicate phases and brezinaite from the Tucson iron. The elements are arranged in order of falling 50% condensation temperature (Lodders 2003), except the REE, which are arranged in order of increasing *Z*. a) Glass inclusions in olivine. Glass is rich in refractory elements and Li but is depleted relative to these elements in Sc, Ti and Nb, and in V, Cr and Mn. b) Clear mesostasis glasses (CMG) and recrystallized mesostasis glasses (RMG). Trace element abundances are very similar to those in glasses of glass inclusions (a) except for CMG-T3, which shows terrestrial contamination (LREE, Sr, Ba, Li). c) Olivines are homogeneous and poor in trace elements. Ol-B4 appears to have a slight terrestrial contamination. Incompatible elements but also V, Cr, and Mn have very low abundances. d) Pyroxenes. The clinopyroxene Cpx B4 has high trace element contents with roughly a solar abundance pattern, except for deficits in Sc, Ti, Nb, Ba, V, Cr, and Mn. The Al-rich enstatites Px-B3 = 9.8, Px-B4 = 9.43, and Px1-B8 = 3.15 (the number after the equal sign indicates the Al_2O_3 content in the pyroxene as measured by EMP), have high trace element contents, which are fractionated with deficits in incompatible elements and V, Cr, and Mn. Al-rich enstatites are variable in their trace element contents, which roughly correlate with the Al content. The Al-poor enstatites Px-B3 = 0.7 and Px2-B8 = 0.84 are very poor in trace elements, in particular the REE, Y, Nb, Sr, Ba, V, Cr, and Mn. The relatively high contents of LREE in Px2-B8 = 0.84 probably originate from terrestrial contamination. e) Anorthite and brezinaite. Anorthite has normal fractionated trace element abundances. Brezinaite is very poor in trace elements but has high contents of Ti, Nb, and V—elements that have low abundances in the silicates.

Table 3. Trace element contents of glass inclusion and mesostasis glasses and host olivine of the Tucson iron meteorite. Secondary ion mass spectrometry data in ppm (wt). Typical errors are approximately 10%, when larger they are given in parentheses in units of the last digit.

	G.I.1	G.I.1 Ol host	G.I.B#5	G.I.B#5 Ol host	CMG-T3	Ol 1-T3	CMG-T4	CMG-B17	Ol- B17	RMG-B1
Li	24.4	0.69	5.09	0.36	35	1.07	20.4	13.6	0.8	14.8
Na	798				135	0.56	941			
K	219		5	2.27	28.4	0.19	502	11.4	0.55	12.8
Ca				904		863		82,105	734	76,456
Sc	4.9	3.53	10	6.51	2.3 (3)	1.08	8	8.3	2.78	9.2
Ti	37	81.3	18.8	18	34	71.9	37	28	66.5	87
V	29.4	14.1	8.3	11.1	7.2	14.7	67	9	12.3	4.1
Cr	503	336.7	140	167	111	360	1780	92.1	226	440
Mn	129				89	35.8	106	72.5	30.9	87.3
Fe	3067				3440	1825		3938	944	6110
Co	9.5				19.5	14.9	785	20	1.84	
Sr	77		50	0.01 (2)	318	0.03	169	91.7	0.05	98.5
Y	13		7.8	0.075	14.3	0.03	8.7	8	0.022	6.7
Zr	34		17.1	0.02 (4)	77	0.02	27	25.5	0.017 (2)	24.6
Nb	0.03 (1)						0.6 (7)	0.007 (2)		0.04 (5)
Ba	32		31.6	0.02 (6)	175	0.007 (2)	58	49	0.03 (4)	58.1
La	1.4		0.95		5.6		1.5 (2)	1.57	0.001 (5)	1.57
Ce	6.2		5.1		18.2		5.7	5.1	0.003 (8)	5.8
Pr	0.81		0.81 (9)		2.3		0.8 (1)	0.63	0.0006 (3)	0.64
Nd	3.7		3.2		9.7		2.9	2.8		2.92
Sm	1.4 (2)		1.0 (2)		3		1	1.01		0.98
Eu	0.40 (5)		0.56 (8)		1.3		0.3 (6)	0.45		0.45
Gd	1.9		1.8 (3)		3.2		1.1 (2)	0.9 (1)		1.04
Tb	0.36		0.32 (6)		0.37 (5)		0.2 (3)	0.15 (2)		0.15 (2)
Dy	2.2		2.2		2.6		1.3	1.39		1.29
Ho	0.41		0.38 (6)		0.54 (6)		0.3 (4)	0.28		0.25
Er	1.12	0.004	1.1		1.56	0.006 (1)	0.67	0.85		0.74
Tm	0.15 (2)	0.001	0.14 (4)		0.16 (3)		0.12 (2)	0.11		0.09 (1)
Yb	0.91	0.019	0.9 (1)		1.2	0.016 (2)	0.9 (1)	0.87	0.008 (2)	0.78
Lu	0.1 (2)	0.005			0.19 (3)		0.12 (3)	0.1	0.003 (1)	0.1

Sc, La, Ce, and Li ($\sim 1 \times$ CI), and very low contents of Y, Ti, V, and Cr ($< 0.1 \times$ CI).

The sulfide brezinaite (Table 4; Fig. 6e) is very poor in lithophile trace elements with most having abundances $< 0.1 \times$ CI, except for Ti, Nb, and V, which have abundances between approximately 8 and 75 $\times$ CI, and Zr, Ba, Mn, and Li (~ 0.5–$5 \times$ CI).

DISCUSSION

The Tucson meteorite has several peculiar features that led to a series of contradicting conclusions reached in previous studies. Among these features is a parallel or subparallel curved aggregate arrangement of its silicate inclusions, which in previous studies (Bunch and Fuchs 1969; Buchwald 1975; Nehru et al. 1982; Prinz et al. 1987) has been interpreted to indicate flow. Because of this apparent flow structure it was suggested that the silicate mass was invaded by shock-melted metal. Similarly, Nehru et al. (1982) proposed a turbulent impact mix of metal and a forsterite-enstatite silicate assemblage at high temperatures ($\sim$1500 °C) that also led to volatilization of Ge and other volatile elements. We shall discuss the arrangement and composition of Tucson silicate inclusions and offer alternative suggestions for their formation and the depletion of Tucson in volatile elements, siderophile as well as lithophile ones.

The microstructure of the metal and its chemical homogeneity has led to the suggestion (Miyake and Goldstein 1974) that the Tucson metal underwent rapid cooling (about 1 °C per 1000 years). Some rapid cooling appears to be necessary for the survival of metastable aluminous pyroxenes and glass in the silicate inclusions. What can be stated right away is that the Tucson constituents and the whole rock must have seen quick cooling from at least the liquidus temperature of the glasses present.

Table 4. Trace element contents of phases of the Tucson iron meteorite. Secondary ion mass spectrometry data in ppm. Typical errors are approximately 10%, when larger, statistical errors are given in parentheses in units of the last digit.

	Coexisting phases			Coexisting phases			Brezinaite		Anorthite	Pyroxene		Olivine
	Ol-B8	Px2-B8 = 0.84	Px1-B8 = 3.15	Cpx B4	Px-B4 = 9.43	Ol-B4	TB13 SC	TB15 CC	T#7	Px-B3 = 0.7	Px-B3 = 9.8	Ol.T#10
Li	1.12	3.21	3.72	9.4	4.29	0.65	5.04	0.12	2.19	0.9	1.68	0.360 (6)
K	1.79	4.22	1.68	10	4.1	0.40 (7)	1.40	0.57	12	2.99	2.47	
Ca	906.7	1853	7349		6789	824	28.4	262.2		1860	8110	844
Sc	1.79	2.99	6.1	9.7	9.1	1.1 (2)	0.116	0.11 (2)	9.2	15.2	16.5	6.97
Ti	163.5	332	996	1730	1207	149	3089	3300	11.4	204	1180	26
V	15.8	8.5	25.6	36	44.7	16.2	3425	3309	0.54	5.33	13.3	10.8
Cr	312.2	419	429	815	1201	354			24.8	272	230	188
Mn	39	58.0	64.4	120	127	38.1	6127	6244				
Fe	1407	1195	2087			2464						
Co	2.03	5.0	13.5			9.4						
Sr	0.029 (4)	0.086 (9)	0.11	159	1.87	0.09 (1)		0.33	98.5	0.038 (7)	0.12 (2)	0.018 (4)
Y	0.027 (3)	0.075	1.03	10	1.34	0.06 (1)	0.0027 (5)	0.028 (6)	0.12 (2)	0.09	1.35	0.029 (4)
Zr	0.025 (4)	0.16	1.42	24.5	3.2	0.10 (2)	1.57	1.2		0.16	2.07	0.011 (4)
Nb		0.0020 (6)	0.005 (1)	0.57	0.049 (6)		8.5	7.6				
Ba	0.033 (6)	0.16 (2)	0.10	3.3	2.1	0.25 (4)	3.52	0.67	32.4	0.06 (1)	0.17 (3)	0.015 (5)
La	0.0008 (3)	0.028 (3)	0.009	2.6	0.040 (5)		0.0048	0.021 (4)	0.26 (4)	0.012 (4)	0.013 (6)	
Ce	0.0025 (6)	0.067 (8)	0.033 (5)	8.4	0.10	0.010 (3)	0.0068	0.049 (9)	0.6		0.08 (2)	
Pr		0.0057 (8)	0.0050 (9)	0.97	0.015 (2)		0.0009	0.007 (2)	0.03 (1)			
Nd		0.014 (2)	0.031	4.5	0.068		0.0093 (5)	0.019 (3)	0.17 (4)		0.03 (1)	
Sm			0.017 (3)	1.54	0.037 (7)		0.0025 (4)	0.006 (3)				
Eu				0.72	0.007 (2)				0.39 (6)			
Gd		0.007 (2)	0.049 (7)	2.0	0.062 (9)						0.12 (3)	
Tb		0.0012 (4)	0.009 (2)	0.23	0.013 (2)						0.03 (1)	
Dy	0.0017 (6)	0.010	0.135	1.8	0.16						0.25 (3)	
Ho	0.0007 (3)	0.0034 (7)	0.032	0.33	0.042 (5)						0.05 (1)	
Er	0.0045 (9)	0.009	0.13	0.97	0.16						0.13 (2)	
Tm		0.0020 (6)	0.021 (3)	0.16	0.027							
Yb	0.013 (2)	0.017 (3)	0.17	0.82 (9)	0.25					0.05 (2)	0.28 (3)	
Lu	0.0029 (7)	0.004 (1)	0.020 (3)	0.07 (2)	0.029 (5)	0.006 (3)					0.03 (1)	

Note: Ol = olivine; Px2-B8 = 0.84: low-Ca pyroxene (0.84 wt% Al_2O_3, EMP); CPX = clinopyroxene.

Additional confusion exists about the forsterite-enstatite silicate assemblage, which has been suggested to be related to enstatite meteorites (e.g., Bunch and Fuchs 1969; Nehru et al. 1982). On the other hand, a study of silicate components in the Bencubbin, Kakangari, Renazzo, and Tucson meteorites found that the silicates share a similar petrology, that they are relatives and represent a similarly reduced chondritic assemblage (Prinz et al. 1987). The oxygen isotopic composition of Tucson silicates—being remarkably similar to that of Renazzo silicates and close to the fractionation line defined by Bencubbin and Kakangari—strongly supports the petrological results and led Prinz et al. (1987) to suggest a common origin for these unique meteorites in a region of the solar nebular undergoing evolutionary changes.

The results of our chemical and petrographic studies support the chondritic connection suggested by Prinz et al. (1987). They also give new evidences for a variety of possible processes that could have created the silicate inclusions and allow us to propose an alternative model for the formation of this particular meteorite and its constituents.

The Paragenetic Sequence

The petrology of the silicate inclusions indicates a paragenetic sequence that begins with olivine as the first mineral to form (±glass). The olivine apparently did crystallize from a silicate liquid (documented by glass inclusions and mesostasis glass), which had a refractory composition as documented by glassy inclusions in olivine. The Ca-Al-Si-rich liquid (glass precursor) is an early phase, that could have predated (e.g., liquid droplet with forsterite completely included; Fig. 2d) and evidently coexisted with forsterite (e.g., primary glass inclusions, Figs. 2b, 2f, and 2h). A particular object is the perfectly round glass droplet that includes a euhedral olivine, a two-phase chondrule-like object (Fig. 2d). There cannot be any doubt that this olivine grew from the liquid that includes it.

Olivine either remained isolated (small silicate inclusions) or aggregated to form small and large, usually elongated, objects. These aggregates also collected grains of the Al-poor, trace element-poor enstatite. The genesis of this enstatite cannot be firmly established but the trace element contents of these pyroxenes, which will be discussed in detail below, indicate that they formed in a highly reduced environment in coexistence with sulfides. The fact that the Al-poor enstatite is a Ca-poor clinopyroxene suggests that it originated from an environment that was slowly cooled below ~600 °C. Al-poor clinoenstatites could be xenocrysts in the Tucson silicate aggregates. Their place of origin likely was similar to that of enstatite meteorites (we shall discuss this in detail below).

Both olivine and low-Al clinoenstatite are embedded in Al-rich orthoenstatite (Fig. 4b), the product of a reaction between early formed olivine and a Si-rich medium (likely a liquid), leaving rounded olivine relics. Such a reaction is commonly observed not only in chondritic constituents, such as chondrules and aggregates (e.g., Varela et al. 2005) but also in other meteoritic matter (e.g., Kurat 1988). However, the orthopyroxene formed in this way is rarely Al-rich. The Al-rich enstatite, as well as Ca-rich clinopyroxene and anorthite, which are associated with it, are late phases (Figs. 4c and 4d). The mineral association Al-rich enstatite + anorthite + clinopyroxene is also frequently accompanied by brezinaite with which these phases form symplectitic intergrowths (Fig. 4c).

The particular growth feature of olivine, which developed crystal faces toward the liquid (=glass; Figs. 2c and 2d) but not toward the metal, clearly indicates that some metal was already present when olivine grew from the Ca-Al-Mg-rich liquid. Because metal is also present inside primary glass-bearing inclusions in olivine (Fig. 2b) and surrounds the silicate inclusions, it must have been present during the formation of most constituents of Tucson. The large, cm-sized elongated metal nodules (“austenite grains” of Buchwald 1975), which are free of silicates but are covered by silicate inclusions (Figs. 1a and 1b), also document the early presence of metal.

The petrographic evidence and the chemical composition of all studied phases that will be discussed below indicate a sequence of formation as follows:

1. Metal nodules (and continuing metal precipitation throughout the whole evolution of the Tucson rock).
2. Al-poor enstatite (xenocrysts [?] formed in a nearby region with affinity to the enstatite meteorite source region).
3. Ca-Al-Mg-Si-rich liquid nucleates from vapor.
4. Forsterite condensation: growth from Ca-Al-Mg-Si-rich liquid (fed by the vapor; the remnant is now Ca-Al-Si-rich glass).
5. Aggregation of forsterite + liquid + Al-poor enstatite.
6. Olivine reacts with increasingly Si-enriched liquid (fed by vapor) and forms Al-rich enstatite.
7. Brezinaite formation (by breakdown of a chemically complex precursor phase, possibly a liquid formed by partial sulfurization of metal?), formation of Al-rich pyroxene, Al-rich diopside, anorthite, and brezinaite—pyroxene symplectites.

The chemical and mineralogical study of silicate inclusions performed by Nehru et al. (1982) shows that

silicate inclusions are composed of 66% forsterite, 30% enstatite, approximately 3% diopside, 0.7% anorthite and glass, and traces of Mg-Al spinel and brezinaite. These authors proposed the following sequence of crystallization: forsterite (being the earliest crystallized mineral)–enstatite–aluminous enstatite ± aluminous diopside–(anorthite + spinel + glass). Their preferred hypothesis for the formation of Tucson considers that the metal and silicate were mixed during an impact at temperatures high enough to produce forsterite and melt (~1500 °C), resulting in evaporation of volatiles elements (e.g., Ga, Ge, and As) from the metal and from the silicates (e.g., Na, K, and Mn). Subsequent rapid cooling allowed survival of metastable aluminous pyroxene and glass. However, the sequence of formation described in this study—based on new petrographic evidences—differs from that of Nehru et al. (1982), as metal and the Ca-Al-Si-rich liquid (glass precursor) are early phases. Apparently, metal (e.g., silicate-free nodules in Fig. 1) was precipitated before and throughout silicate formation and aggregation, and some of the early silicate products were trapped by the metal and became isolated. In this way, products of all evolutionary steps were preserved. The very simple, small, round olivine plus glass objects are the products of the earliest step of silicate formation.

Chemical Composition of Silicates

Major Elements in Silicates

The previous study of Tucson by Prinz et al. (1987) arrived at the result that the Tucson silicates are related to carbonaceous chondrite constituents. They were identified to be the most extreme examples of highly reduced and volatile-element-depleted assemblages among the meteorites investigated (Renazzo, Bencubbin, and Kakangari). Major element compositions of silicates obtained in our study fully support these previous findings. However, a detailed comparison of the analyses reveals that olivine is on average the most FeO-poor silicate, with the lowest FeO content encountered being approximately 0.19 wt%. The FeO-poor olivine coexists with pyroxenes and glass, which contain about the same and commonly more FeO than the olivine. Because Tucson has experienced widespread weathering, oxidized Fe is distributed in silicate grain boundaries and cracks, resulting in increased Fe signals during EMP analysis. Analysis of carefully selected sites nevertheless revealed that pyroxenes, glass, and olivine are not in chemical equilibrium with respect to Fe distribution. The chemical disequilibrium between coexisting phases becomes obvious if one looks at the highly variable chemical composition of pyroxenes. The morphologically distinct Al-poor clinoenstatites, which are enclosed by Al-rich pyroxenes, are also poor in Fe, Ti, Cr, Mn, and Ca. They are neither related to the olivines nor to the Al-rich orthoenstatites and appear to be xenocrysts.

The Al-rich orthopyroxenes have highly variable compositions within and among grains, with Al_2O_3 contents ranging up to 18 wt%. Morphologically they appear to have formed from earlier olivine, which they now poikilitically enclose. Compared to the Al-poor clinoenstatite, the newly formed pyroxenes are richer not only in Al but also in Ti, Cr, and Ca. Apparently, the olivine first grew from a liquid and then reacted with it to form Al-rich enstatite. Pyroxene formation by reaction between olivine and a Si-rich liquid has been documented in constituents of many chondrites. However, the reaction product usually is an ordinary low-Ca pyroxene, orthopyroxene, or clinopyroxene. The formation of aluminous enstatite could be the result of very fast cooling—as has been suggested by Nehru et al. (1982). Small amounts of aluminous diopside and anorthite apparently grew in the very same event.

Tucson seems to contain silicates from two different sources. Both types of silicates come from highly reduced environments and from environments very poor in volatile elements. A relationship to constituents of C chondrites appears to be likely.

Chemical Composition of Glasses

The chemical composition of the glass inclusions in olivine and of mesostasis glass (Figs. 2b–h) contains valuable genetic information. Glasses at different locations give information related to different evolutionary steps during formation of the silicate inclusion. On the one hand, the glass inclusions are in contact only with the host phase olivine and retain information related mainly to conditions prevailing during growth of this phase (e.g., Kurat et al. 1997; Varela et al. 2002, 2003, 2005). On the other hand, the mesostasis glasses, commonly in contact with several phases and also open to the environment, reveal some hints about the conditions prevailing during late events (e.g., Varela et al. 2003, 2006; Varela 2008).

The perfectly round glass droplet that includes a euhedral olivine (Fig. 2d) can provide information about the chemical composition of the initial liquid. There cannot be any doubt that this olivine grew from the liquid that includes it. Viewed from an igneous point of view, the object formed from an all-liquid droplet. An estimate of the percentage for the constituent phases (e.g., by point counting: a total of 1100 points of which 720 are on olivine) gives: olivine 65%, glass 35%. The estimated bulk composition of the all-liquid droplet is: SiO_2, 44.7 wt%; MgO, 38.2 wt%; Al_2O_3, 10.5 wt%; and CaO, 6.2 wt%, with minor FeO,

0.39 wt%. Although this is a rough estimate as the percentage of constituent phases of this type of objects in Tucson can vary (~50–80% olivine), in order for the forsterite to have grown from an initially all-liquid droplet, the chemical composition of that liquid must have been highly refractory and very rich in olivine component (e.g., a CaO-MgO-Al_3O_2-SiO_2 [CMAS] liquid)—which implies a very high temperature (> ~1700 K, e.g., Nehru et al. 1982).

Also, if the mesostasis glass is a residual melt, its composition will change as crystallization of different phases proceed. According to Nehru et al. (1982), the silicate minerals in Tucson formed from a high-temperature melt (between 1300 and 1500 °C), with olivine crystallizing first, followed by enstatite and aluminous pyroxenes. If this is so, the mesostasis should differ in its chemical composition from the glass trapped in the early phases (e.g., primary glass inclusions in olivine). GIs in Tucson olivine have higher SiO_2 (54–57 wt%), lower Al_2O_3 (21–24.9 wt%), and similar contents of CaO (17.6–19.2 wt%) than the mesostasis glass (48.1–49.7 wt% SiO_2; 25.3–28.3 wt% Al_2O_3; 17.4–20.1 wt% CaO). The high content of SiO_2 commonly observed in glass inclusions in olivine could be the result of a suppressed reaction of the liquid with olivine to form enstatite. Variations in the contents of major elements in inclusion and mesostasis glass exhibit a trend opposite to that expected for an igneous crystallization sequence. The residual melt after crystallization of Al-rich phases (e.g., Al-rich enstatite, Al-rich diopside, and anorthite) should have a lower and not higher Al_2O_3 content than the original melt (Tables 1 and 2). Similarly, the CaO content of the mesostasis glass should be low after crystallization of diopside and anorthite. However, both types of glasses have similar CaO contents. Apparently, glasses in Tucson do not simply record crystallization of olivine followed by a reaction of the early olivine with residual liquid. Some additional process(es) must have occurred during the formation of Tucson silicate inclusions. This feature is also reminiscent of C chondrite constituents such as chondrules and aggregates (e.g., Varela et al. 2002, 2005).

Trace Elements

Minerals. All olivines appear to have very similar trace element contents. Their abundance pattern is highly fractionated (Fig. 6c) and almost in crystal-chemical equilibrium with the coexisting liquid (glass). The distribution of trace elements between olivine and coexisting glass closely follows the experimentally determined distribution coefficients (Fig. 7) with four notable exceptions: La and Ce, Ti, and V. The high abundance of the highly incompatible elements La and Ce in olivine could be the result of terrestrial contamination, which is also evident in many other minerals (see below and Fig. 8) and glasses. However, the discrepancy of the abundance of Ti between that found and that predicted is very large (> 100×) and beyond any possible error. The high distribution values for Ti and V—results of very low abundances in glass—indicate that olivine is not in equilibrium with its coexisting glass inclusion or mesostasis glass. Because most other elements do behave very well, the petrographic finding that olivine grew from the liquid it now carries as a glass inclusion is strongly supported. Apparently, Ti was removed from the liquid = glass after the olivine formed and re-equilibration was not possible (fast cooling). We shall encounter this phenomenon also when looking at the other silicates in Tucson. This loss of Ti is probably related to the formation of brezinaite, which scavenged Ti, Nb, and V (Fig. 6e). Consequently, also the abundance of V in olivine deviates from chemical equilibrium with coexisting glass.

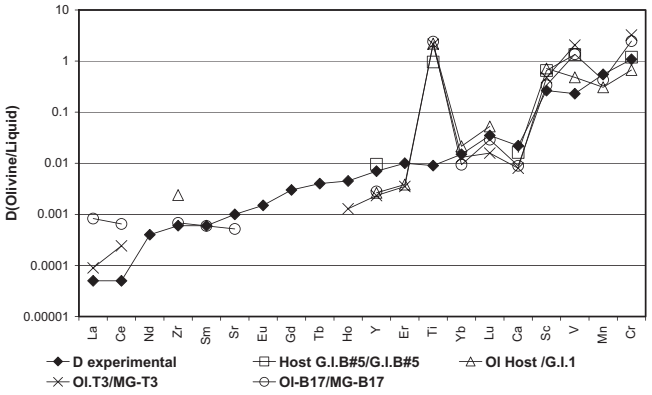

Fig. 7. Distribution of trace elements between coexisting olivine and glass in Tucson silicate inclusions compared to experimentally determined olivine-liquid distribution coefficients (black diamonds: Green 1994 [D_{La}: 0.00005, D_{Ce}: 0.00005, D_{Sm}: 0.0006, D_{Ho}: 0.0045, D_{Yb}: 0.015, D_{Lu}: 0.035], McKay and Weill 1977 [D_{Sc}: 0.265, D_{Cr}: 1.08], Kennedy et al. 1993 [D_{Zr}: 0.00068, D_{Sr}: 0.0015, D_{Y}: 0.006, D_{Ti}: 0.016, D_{Ca}: 0.022, D_{Er}: 0.013, D_{V}: 0.27, D_{Mn}: 0.55]). Olivines in Tucson are close to chemical equilibrium with their coexisting liquid, except for Ti and V, and La and Ce in some samples. The abundance anomalies in La and Ce could be due to terrestrial contamination.

In contrast to olivine, pyroxenes in Tucson are compositionally very inhomogeneous, both in major and trace elements. Aluminum-rich orthopyroxenes are rich and Al-poor clinopyroxenes are poor in refractory trace elements (Fig. 6d). The differences span about 1.5 orders of magnitude. The abundance patterns are fractionated, indicating chemical exchange reactions attempting equilibration with a vapor, liquid, or solid

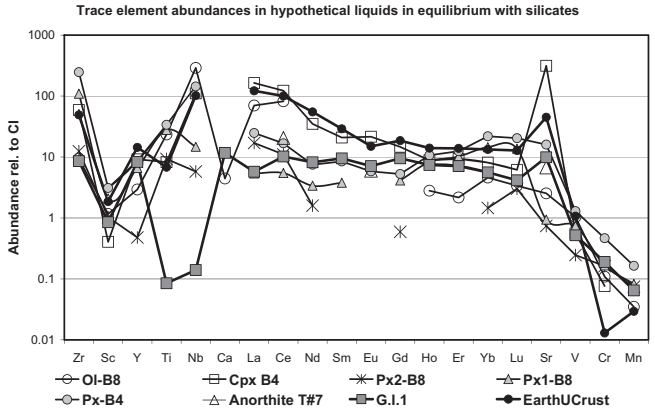

Fig. 8. Trace element abundances in hypothetical liquids in equilibrium with olivine, Al-poor and Al-rich enstatite, Ca-rich pyroxene, and anorthite in Tucson silicate inclusions compared with those of Tucson glass inclusion in olivine (liquid) and the Earth's upper crust (Taylor 1992). The trace element contents in Tucson silicates indicate derivation from a liquid with refractory trace element abundances of approximately $10 \times$ CI and deficits in Sc and moderately volatile and volatile elements. Exception is the Al-poor clinopyroxene Px2-B8, which indicates derivation from a liquid with refractory element abundances of approximately $1 \times$ CI (REE, Y, and Sc)—evidence for its foreign origin. Positive anomalies of Zr, Nb, LREE, and Sr (in particular Cpx B4, Ol-B8) are probably caused by terrestrial contamination. (Distribution coefficients for olivine-liquid as indicate in Fig. 6, for orthopyroxene-liquid: Green 1994 [D_{La}: 0.006, D_{Ce}: 0.008, D_{Eu}: 0.017, D_{Yb}: 0.06]; Kennedy et al. 1993 [D_{Zr}: 0.0033, D_{Sc}: 0.63, D_{V}: 0.61, D_{Cr}: 0.97]; for clinopyroxene-liquid: Zajacz and Halter 2007 [D_{Zr}: 0.105, D_{Sc}: 4.11, D_{Y}: 0.698, D_{Ti}: 0.481, D_{Nb}: 0.02, D_{Yb}: 0.625, D_{La}: 0.067, D_{Ce}: 0.114, D_{Nd}: 0.285, D_{Eu}: 0.6, D_{Gd}: 0.685, D_{Yb}: 0.625, D_{Lu}: 0.486, D_{Sr}: 0.065, D_{V}: 1.14], for anorthite-liquid: McKay and Weill 1977 [D_{Ce}: 0.047, D_{Eu}: 1.2, D_{Sr}: 1.87].)

(e.g., rock) system. Calculation of the composition of a theoretical liquid in equilibrium with the Ca-poor, Al-rich pyroxenes reveals that this liquid must have had refractory trace element abundances of around $10 \times$ CI abundances (Fig. 8). Exceptions are Sc, V, and Cr, which were present at lower abundances, and Zr and Nb, which had apparent abundances of approximately $100 \times$ CI. The deficit in Sc ($\sim 0.1 \times$ Ti) is a marker carried by all silicate phases present in Tucson and, consequently, also the bulk rock. It is the only missing refractory lithophile element in Tucson and because we did not encounter a phase that could have scavenged Sc, we suspect that a refractory phase rich in Sc had removed it from the vapor or the liquids from which Tucson silicates formed.

The trace element abundances of a liquid in equilibrium with Al-poor clinopyroxene appear to be very low and indicate an environment that was quite different from that of the major silicate phases in Tucson (Figs. 6d and 8). Yttrium and the HREEs had abundances of approximately $< 1 \times$ CI, suggesting an environment similar to that from which enstatite meteorites originated.

Trace elements in Tucson Ca-rich clinopyroxene also indicate derivation from a liquid with refractory element abundances of approximately $8–20 \times$ CI, with depletions in Sc, V, and Cr and enrichments in Zr, Nb, La, Ce ($\sim 100 \times$ CI), and Sr ($\sim 300 \times$ CI). These positive anomalies observed in mineral and glasses very likely are due to terrestrial contamination because they are common terrestrial crustal elements and dominantly show up in the smallest grains we analyzed. The very high Sr signal could originate from the desert environment from where Tucson was recovered.

The few data points we have for anorthite also indicate a liquid of about $7 \times$ CI trace element abundances and a slight terrestrial contamination similar to that of olivine (Ce; Fig. 8).

In summary, all silicate phases in Tucson apparently grew from a silicate liquid that had refractory trace elements at approximately $6–20 \times$ CI abundances with nonfractionated (solar) pattern, except for Sc, which was present at low level ($\sim 1 \times$ CI).

Glasses. If the mesostasis glass is a residual phase, we expect its trace elements to be fractionated after crystallization of Al-rich phases with variable REE abundances. However, surprisingly, GIs in olivine as well as the mesostasis glasses have similar contents of refractory trace elements (Figs. 6a and 6b) and have an unfractionated abundance pattern (except for Sc, Ti, and Nb).

The abundances of most refractory lithophile elements are between 6 and $10 \times$ CI, with the exception of Sc, Ti, and Nb, which are depleted.

If the available olivine/liquid partition coefficients for Sc are taking into account (D_{Sc}: 0.265, McKay and Weill 1977; D_{Sc}: 0.12 and 0.15, Kennedy et al. 1993), the host olivine of glass inclusions, G.I.1 and G.I.B#5 (G.I.1 Ol host and G.I.B#5 Ol host), will require coexisting liquids with higher contents of Sc (e.g., $2.3 \times$ CI–$5.08 \times$ CI for G.I.1 Ol host and $4.22 \times$ CI–$9.33 \times$ CI for G.I.B#5 Ol host) than those present in the liquid trapped during their growth (Sc in G.I.1: $0.85 \times$ CI, in G.I.B#5: $1.71 \times$ CI).

The liquid from which olivine grew (e.g., entrapped as primary glass inclusions) apparently had a Sc deficit. This signals fractionation via a refractory phase that scavenged Sc before the liquid formed. In a cosmochemical setting, this indicates early condensation of a highly refractory phase, such as corundum, hibonite, and perovskite. Nehru et al. (1982) report rare Al spinel, which we did not

encounter and Ebel (2006) predicts grossite, perovskite, and Al spinel as high-T condensates at a total p of about 1 bar. The deficits in Ti and Nb seem to support the involvement of perovskite. However, as we have discussed above, Ti and Nb have apparently been removed by brezinaite, because all silicates indicate crystallization from liquids without Ti and Nb deficits (Fig. 8). These elements apparently became chalcophile during the later stages of evolution of Tucson, moved out of the glass and entered brezinaite (together with V and Cr, see Fig. 6e). The two orders of magnitude deficits in the abundances of Ti and Nb in all Tucson glasses (but not minerals!) support loss of these elements from glasses after silicate formation. Apart from the mismatch of Ti and Nb abundances between theoretical liquids in equilibrium with Tucson silicates and the liquids (glasses) present, the match is almost perfect (Fig. 8).

In summary, Tucson silicates crystallized from a liquid of the composition of the glasses present (refractory trace element abundances of approximately $10 \times$ CI)—inclusive the deficits in Sc and moderately volatile and volatile elements—but with the full share of Ti and Nb. The positive anomalies in Zr, Nb, LREE, and Sr obtained for theoretical liquids very likely are the result of terrestrial contamination—in a desert environment.

Because the major and trace element chemical composition of glasses is not akin to that expected during an igneous crystallization sequence and because the abundance of trace elements in all glasses appears to be governed by cosmochemical—rather than a geochemical—fractionation, the widely accepted igneous model for the formation of silicate inclusions in the Tucson meteorite needs to be revised.

Comparison of Silicate Phases: Tucson, CR Chondrites, and Enstatite Meteorites

The Major Elements in Glasses

Considering that the Tucson silicate inclusions are related either to enstatite (Nehru et al.1982) or CR chondrites (Prinz et al. 1987), and considering that glasses can keep a memory of their birth place, we compare elemental compositions of glasses from the Tucson meteorite with those of primary glass inclusions from enstatite meteorites and CR chondrites (Figs. 5a–f). The Ca-Al-Si-rich glasses in Tucson have approximately chondritic Ca/Al ratios and share this property with glasses in carbonaceous chondrite constituents (chondrules and aggregates). With respect to the CaO, Al_2O_3, and SiO_2 contents, Tucson primary glass inclusions matched the Al-poor CR glasses while the CMG is slightly enriched in Al_2O_3 as compared to the Al-rich CR glasses (Figs. 5b and 5c). They also share with these glasses the low CaO contents of their host olivines (~0.13 wt% in Tucson and 0.19 wt% for Al-poor CR glasses). In addition, they part with CR glasses the lack of alkali elements (Fig. 5f). However, the very low contents of TiO_2 in Tucson glasses match those from enstatite chondrites (Fig. 5e). Glasses of primary glass inclusions in enstatite chondrites and achondrites (e.g., Happy Canyon and Northwest Africa [NWA] 1235) have very low contents of CaO (< 1.5 wt%; Fig. 5b), very high contents of SiO_2 (70–80 wt%; Fig. 5d) and are rich in alkali elements (e.g., $Na_2O + K_2O$: 3.8–9.5 wt%; Fig. 5f) (Varela et al. 1998). Clearly, glasses in Tucson differ from those in E meteorites in their Ca, Al, and Na contents.

Thus, if we take into account some of the glass features (e.g., major element composition, elemental ratios such as Ca/Al, Si/Al), the Ca-Al-Si-rich glasses in Tucson resemble those of carbonaceous chondritic silicate assemblages, except for the Ti content. This parentage line is also supported by oxygen isotopes (Prinz et al. 1987).

Trace Elements in Glasses

Our studies of trace elements in glasses of glass inclusions and mesostasis in a variety of meteorites (e.g., Varela et al. 2002, 2003, 2006; Kurat et al. 2003, 2007) have revealed another particular feature of this phase: Despite the differences in major element compositions, all glasses have a very similar trace element abundance pattern that is suggestive of vapor fractionation. Glasses in the Tucson silicate inclusions show also the same unfractionated pattern (Figs. 6a and 6b), with high refractory element and low moderately volatile and volatile element abundances. In addition, this abundance pattern matches those observed in glasses hosted by olivines and mesostasis in constituents of CR carbonaceous chondrites (e.g., Fig. 9), with the exception of Ti and Nb, which are depleted in Tucson glasses, as discussed above (Fig. 6e).

Glasses of glass inclusions in enstatites of the enstatite achondrite NWA 1235 share similar negative abundance anomalies in Nb and Ti with glasses in Tucson. They also have comparable abundance and variation in the moderately volatile elements. However, the contents of refractory elements and REEs are three orders of magnitude lower (e.g., $Y \sim 0.01 \times$ CI) (Fig. 9b) and the volatile elements up to four orders of magnitude higher in enstatite meteorite glasses than in CC, achondrite, and Tucson glasses.

We conclude that Tucson glasses share not only most features with glasses (liquids) from C chondrite constituents but also a few (Ti and Nb depletions) with E meteorite glasses. We interpret these features to

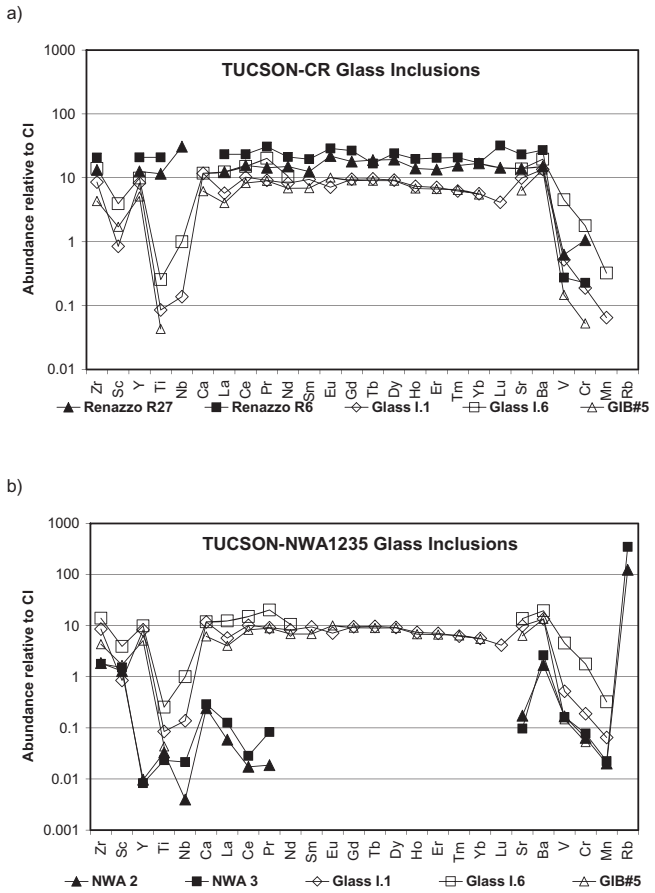

Fig. 9. CI-normalized (Lodders and Fegley 1998) trace element abundances in glasses of Tucson silicate inclusions compared with those in (a) Renazzo (CR; Varela et al. 2002) and (b) NWA 1235 (aubrite, Varela, unpublished data). Tucson glasses are similar to Renazzo glasses but have deficits in Ti, Nb, V, and Cr, which indicate an increased sulfur fugacity. Enstatite meteorite glasses also show this feature but are in addition also very poor in REE and Sr, elements which become chalcophile under strongly reducing conditions with very high S fugacity.

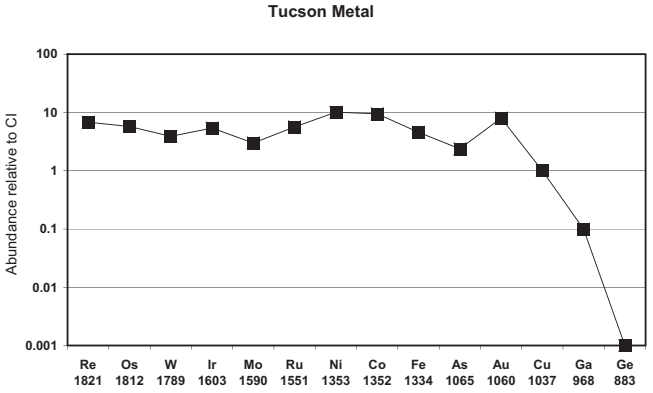

Fig. 10. Siderophile and chalcophile trace elements in Tucson metal (Koblitz 2003) normalized to CI (Anders and Grevesse 1989). Elements are arranged in order of decreasing 50% condensation temperature (at 10^{-4} bar) in K (Lodders 2003), which are shown below the element's symbol. The lower limit of Tucson's metal condensation temperature can be estimated from the fact that Au seems to be fully condensed whereas Cu is not—due to its lower T_c or its chalcophile behavior, or both? Note the slightly lower abundances of Mo, As, and Cu as compared with those of highly siderophile elements (Re, Os, Ir). This could be due to competition from sulfide species in the gas or condensed sulfides, whereas the low abundances of Ga and Ge seem to be related to their low T_c, or both.

indicate an origin in an environment akin to that in which C chondrite constituents formed, but with redox conditions between those for CR chondrite constituents (reducing) and E meteorites (highly reducing and S-rich)—in accordance with the conclusion reached by Prinz et al. (1987).

Tucson Metal and Bulk Composition

The high and unfractionated content of refractory siderophile elements in Tucson metal (Wänke et al. 1983) also indicates a primitive source, highly reducing conditions (high Cr and Si contents), high S fugacity (W, Mo, As, and Cu anomalies), and a possible origin by condensation from the solar nebula gas (Fig. 10, and discussion below). The high Ni/Fe and Co/Fe ratios of the Tucson bulk metal indicate early, high-temperature condensation from the solar nebula in agreement with calculations (e.g., Grossman and Olsen 1974). The W and Mo abundance deficits cannot indicate oxidizing conditions caused by high O fugacity, as has previously been found for Calcium-aluminum-rich inclusions (Fegley and Palme 1985). On the other hand, high S fugacity can also provide e^--scavenging conditions, which have the same effect.

Tucson bulk silicate inclusions (plus sulfides) have approximately chondritic abundances of the refractory lithophile elements at about 1 × CI (Wänke et al. 1983). However, the moderately volatile and volatile lithophile elements are strongly depleted, which excludes an origin of the silicates from an enstatite meteorite parent, but supports a relationship with CR chondrite constituents, such as aggregates and chondrules.

Application of a New Genetic Model

Here, we offer an alternative view for the formation of the Tucson silicate inclusions by following the primary liquid condensation (PLC) model (Varela et al. 2005; Varela and Kurat 2006, 2009). In our study of glasses in chondritic and achondritic meteorites, we found that glasses do not show the chemical signature expected to result from crystallization of the minerals

they are associated with. This particular feature cannot be reconciled with the currently entertained genetic models, which consider them to represent residual liquids of the object's bulk melt (after crystallization of main minerals; Varela et al. 2005, 2006; Engler et al. 2007). The PLC model proposes that crystals are not precipitation products of a liquid with the chemical composition of the bulk object—as in an igneous system—but that they are growing from the vapor with the help of a liquid (the glass precursor) by a process known as vapor–liquid–solid (VLS) condensation (Varela et al. 2005; Varela and Kurat 2009). The liquid layer facilitates ordered growth of the crystal and acts as an accommodation surface because of its large accommodation coefficient (Givargizov 1987). Consequently, those elements that will not easily enter the structure of the olivine, such as Ca, Al, and REE, will be concentrated in the vapor–crystal–liquid interface. This growth mechanism maintains chemical equilibrium between the growing crystal and the liquid as well as between the liquid and the vapor. Recent experimental results by Kobatake et al. (2008) show that forsterite can grow from highly supersaturated silica vapor. The amorphous surface layer of the forsterite illustrates that a liquid phase can condense from the vapor, even under conditions where crystalline forsterite is stable, supporting that the VLS mechanism, as envisage by the PLC model, plays an important role. Also, the recent experimental work undertaken by Toppani et al. (2006) shows that the amorphous boundary layer between gas and crystal has a chemical compositions usually enriched in the elements which do not enter in large amounts into the host crystals (e.g., Si-rich rim for spinel), giving additional support to the PLC model.

Because the liquid is in chemical equilibrium with a large gaseous reservoir, it does not change its composition according to chemical partitioning of elements between growing crystals and liquid but rather according to any compositional change of the vapor. The latter should be much less dramatic than the former and it is therefore expected that glasses show no signal of geochemical fractionation, as it is observed. Recently, this nonigneous formation model for glasses has received support from oxygen isotopic analysis of CV and CR aggregates and chondrules (Jones et al. 2004; Chaussidon et al. 2008). The isotopic disequilibrium found by these authors in coexisting olivine, pyroxene, and glassy mesostasis led Chaussidon et al. (2008) to conclude that pyroxene grains are not comagmatic and that the glassy mesostasis is not the residual parent liquid of the olivine. However, these authors did not consider the solid–gas elemental exchange processes that left omnipresent traces in all meteoritic rocks (e.g., Kurat 1988). Nevertheless, these new results support the PLC model, which proposes that glasses represent quenched liquid samples of the first major phase to condense in the solar nebula and that they record early, primitive (condensation) features as well as late ones from liquid/solid–gas elemental exchange (Kurat 1967; Grossman and Olsen 1974; Varela et al. 2005, 2006; Varela and Kurat 2009). Based on these concepts, we will focus our attention on the glasses with the aim to reveal some new aspects related to the formation of silicate inclusions in Tucson.

Formation of Tucson Silicate Inclusions

As we have discussed above, the chemical composition of glasses is not that expected for a residue left after crystallization of minerals. The Ca-Al-Si-rich liquid represented by the glasses appears to be a relative of the initial Ca-Al-Mg-Si-rich liquid that initiated the silicate crystallization sequence. The formation of the silicate inclusions in Tucson is here discussed in the light of the PLC model (summary in Varela and Kurat 2009).

An SiO_2 versus Al_2O_3 plot shows that glasses in chondritic objects define a trend connecting two extreme compositions, a refractory Ca-Al-rich and a Si-rich one. This chemical variation is due to an important evolutionary process, namely addition of Si to the object growing from the nebula (e.g., Varela et al. 2005; Libourel et al. 2006). The PLC model proposes that the primary Ca-Al-(Mg)-rich liquid is a precondition for the condensation of the major silicates from the solar nebula. The existence of such a liquid is predicted by condensation calculations in a ''dust-enriched'' solar nebula (e.g., Yoneda and Grossman 1995; Ebel and Grossman 2000; Ebel 2006; Boesenberg and Ebel 2009) and in a high-p solar nebula (Ebel 2006). From this liquid crystallizes olivine, which stays either isolated (Figs. 2b–d), forms irregular aggregates (Figs. 4a and 4b), and, if enough liquid is available, they form two-phase droplets (Figs. 2c and 2d and in chondrites, Varela and Kurat 2006, 2009). As the composition of the nebula evolves, the composition of the liquid in equilibrium with the solar nebula gas adapts and the Si content increases, reflecting the increased Si activity in the vapor. This leads to the formation of low-Ca pyroxene by the reaction of the Si-enriched liquid with the previously precipitated olivine (e.g., Varela et al. 2005; Libourel et al. 2006):

$$Mg_2SiO_4(\text{solid}) + SiO_2(\text{liquid, gas}) \leftrightarrow 2MgSiO_3(\text{solid}). \quad (1)$$

Traces of this reaction can be found in chondritic constituents of all chondrite classes and in constituents

of many achondrites. In the case of Tucson, this reaction took place within a short time and led to the formation of the unusually Al-rich orthoenstatite. Fast cooling apparently prevented the formation of Al-poor enstatite + anorthite assemblage. Thus, the two early components of the silicate inclusions in Tucson can form in this way: a Ca-Al-Mg-rich primary liquid condensed from the solar nebula and helped to grow olivine by the VLS process. We have previously shown for chondritic meteorites, that if olivine is a primitive high-Ca olivine and the glass keeps its pristine composition (e.g., Ca-Al-rich with Ca/Al chondritic ratio), then both phases are in equilibrium with respect to their CaO contents (Varela et al. 2005; Varela and Kurat 2009). This suggests that these olivines crystallized from a liquid with the chemical composition of this particular GI (Weinbruch et al. 2000; Varela et al. 2002; Pack and Palme 2003). However, in the Tucson meteorite, the Ca distribution partitioning between olivine and glass—that deviate from equilibrium conditions in the CMAS system (Libourel 1999)—could indicate re-equilibration under subliquidus conditions. Similar to what have been observed in CR chondrites (Varela et al. 2002). Subsequently, increased Si activity in the nebular gas led to the reaction of this olivine with the evolving liquid and to the formation of Al-rich and trace element-rich enstatite and small amounts of Ca-rich clinopyroxene and anorthite. Toward the end of this reaction also brezinaite formed—possibly not directly as brezinaite but rather as a Cr, Mg, and S-rich phase (liquid? see below), which subsequently reacted with the primary liquid and broke down to brezinaite + Al-rich enstatite, resulting in the brezinaite-Al-enstatite symplectites as well as Al-rich diopside and anorthite.

The variable chemical compositions of glasses also indicate that conditions changed between the crystallization of the olivines and the formation of Al-rich enstatite.

Despite the fact that the primary glass inclusions in olivine have Al_2O_3 contents around 22 wt%, the CMG (which is expected to keep a record of the latest prevailing conditions) has a higher Al_2O_3 content (mean around 28 wt%) (Fig. 5a). Interestingly, both types of glasses have similar abundances of trace elements with patterns suggesting vapor fractionation (Figs. 6a and 6b). The high variability in the Al_2O_3 content observed among and within pyroxene crystals has previously been considered to be the result of a metastable state of the pyroxene because of the difficulty of nucleating feldspar in a dry and rapidly cooling assemblage (Nehru et al. 1982). According to this view, the presence of metastable aluminous pyroxene as well as the feldspatic glass point toward rapid cooling of the system. However, the Al-Ca-Si-rich liquid (precursor of the glass that actually formed primary glass inclusions and mesostasis) appears to have had enough time to achieve equilibrium with the coexisting forsterite (at high *T*), as demonstrated by the forsterite/liquid trace element distribution coefficients (Fig. 7), which approach experimentally determined values (McKay and Weill 1977; Kennedy et al. 1993; Green 1994).

The positive abundance anomalies of Ti and V could be a consequence of changing conditions, which changed the geochemical character of these elements from lithophile to chalcophile. Consequently, they were sequestered into coexisting brezinaite (Fig. 6e) after olivine precipitation and pyroxene formation, leaving the glass very poor in Ti and V.

Thus, nebular cooling seems to be recorded in Tucson until formation of a Cr-rich sulfide liquid. Highly "dust-enriched" solar nebula condensation models predict FeS precipitation at about 1400 K (for $1000 \times$ CI dust enrichment; Ebel 2006), with no possibility of Cr sulfides to form under such oxidizing conditions. Interestingly, none of the published models predicts precipitation of Cr-rich sulfides. As of today, we are left with the choice of coprecipitation of CaS with Cr_3C_2 under highly reducing conditions (C/O > 1.5; Ebel 2006). However, Tucson presents clear evidence for the precipitation of a complex (liquid?) sulfide phase (Cr, Mg, S liquid), which cooled and finally led to the formation of the ubiquitous Al-rich enstatite-clinopyroxene-anorthite-brezinaite assemblage (Figs. 3a–c, 4c, and 4d). The symplectitic texture of this assemblage indicates break-down of such a sulfide liquid or solid (glass?). A possible scenario could be: Cr condenses into Fe-Ni metal (Grossman and Olsen 1974), gets in part oxidized by high S fugacity and forms CrS, which also takes up V, Ti, Al, Mo, Mg, W, and separates from metal as a liquid (e.g., Mitsui et al. 2002), which probably contains mainly CrS and MgS. It reacts with silicate liquid or glass:

$$\underset{\text{(sulfide)}+}{MgCrS_2(l)} + \underset{\text{(silicate)}+}{SiO_2(l,g)} + \frac{1}{2}\underset{\text{(gas)}}{O_2(g)} = \underset{\text{(pyroxene)}+}{MgSiO_3} + \underset{\text{(sulfide)}}{CrS_2} \quad (2)$$

The missing O could come from the gas or from conversion of TiO_2 to TiS_2 in the liquid/glass. Subsequently, CrS_2 reacts with CrS

$$CrS_2 + 2CrS = CrCr_2S_4 \quad (3)$$

and forms brezinaite. The final products of these processes are brezinaite and low-Ca pyroxene. The latter takes up Al available from the silicate liquid and is quickly chilled to Al-rich orthopyroxene. The diffusive transports necessary in these reactions led to

symplectitic intergrowths of the final products, brezinaite and Al-rich enstatite. These reactions must have taken place at high temperature before FeS became stable and reacted with brezinaite to form daubreelite (e.g., Balabin et al. 1986).

The refractory and reduced silicates of the Tucson iron are embedded in a refractory metal, which has high and almost unfractionated abundances of refractory siderophile elements at approximately 3–9 × CI, low contents of volatile siderophile elements (Fig. 10), and high contents of Si and Cr (e.g., Wänke et al. 1983). Trace element abundances in Tucson metal also are governed by volatility (as they are in glasses). An origin by direct condensation from solar nebula gas seems to be likely. Such an origin has been also favored by previous investigators of "relatives" of Tucson, such as Bencubbin and Allan Hills 85085 (e.g., Newsom and Drake 1979; Weisberg et al. 1990; Meibom et al. 1999; Campbell and Humayun 2004).

Metal nuggets (Fig. 1a) could represent early precipitated droplets, which collected silicates at their surface (also noted by Buchwald 1975). Early olivine contains metal droplet inclusions (Fig. 2b)—as do CM chondrite olivines (e.g., Grossman and Olsen 1974). Olivine growth was occasionally hampered by metal in contact with the liquid droplet (Fig. 2c) and metal surrounds early formed silicate objects and in this way preserved valuable information on the early stages of Tucson's genesis. Apparently, metal precipitated before and contemporaneously with the silicates—as is predicted by theoretical condensation calculations for a gas of solar composition (e.g., Ebel 2006). Tucson apparently obeys the theoretical phase diagram for high-p condensation of a gas of solar composition (Ebel 2006), according to which metal condenses before olivine. By contrast, most chondrite constituents record predominantly primary silicate precipitation with late addition of metal (e.g., Varela et al. 2005, 2006; Varela and Kurat 2006, 2009)—as predicted by the condensation behavior of highly "dust-enriched" solar nebula gas (e.g., Ebel 2006) where olivine condenses before metal. Apparently, Tucson recorded formation of meteoritic matter under high p_{tot} ($\sim > 1$ bar) and high T ($\sim > 1800$ K) conditions in the solar nebula—as do CR, CB, and CH chondrite constituents.

The silicates plus sulfide sample of Tucson analyzed by Wänke et al. (1983) is very rich not only in V and Cr but also in Mo ($\sim 1 \times$ CI), Ir ($0.3 \times$ CI), and Ni ($\sim 0.1 \times$ CI). This apparently is a consequence of the chalcophile behavior of these elements under the prevailing conditions. The high abundance of Ir could also possibly be due to its chalcophile character, but we do not know its abundance in Tucson sulfides. An alternative explanation is the possible presence of refractory metal nuggets in the separated silicate plus sulfide sample of Tucson. Such nanonuggets appear to be very common in all chondritic silicates: Chou et al. (1973) found apparent metal/silicate distribution coefficients for Ir of only approximately 50 instead of the experimentally determined $> 10^{12}$ (Borisov and Palme 1995) for 1300 °C and $\log(fO_2)$ = IW-2. Furthermore, Rambaldi (1976) found that Ir is concentrated in the fine-grained metal fraction of chondrites. Very small highly siderophile element metal grains seem to be abundantly present in chondrites (and other meteoritic silicates). Whether these nuggets are residuals from solar nebula dust evaporation or early condensates is still a matter of debates (Chou et al. 1973; Rambaldi 1976; Berg et al. 2009). Tucson apparently collected such refractory nuggets—another feature connecting it to chondrites.

The Cr content of Tucson silicates is very low, approximately 100–500 ppm in clean glasses and olivines. Combining these values with the Cr content of the Tucson metal (1540 ppm; Wänke et al. 1983), we arrive at Cr distribution coefficients between silicates and metal of $D_{Cr}^{S\text{-}M} \sim 0.065$–$0.325$. The linear relationship between $D_{Cr}^{S\text{-}M}$ and pO_2 as experimentally determined by Rammensee et al. (1983):

$$\log D_{Cr}^{S-M} = 0.643 \log pO_2 + 6.85 (\text{for} T = 1600^\circ\text{C}) \quad (4)$$

allows us to estimate $\log pO_2$ and we obtain a range from −11.4 to −12.5 atm at T = 1600 °C. This is low enough to also partition most of V into the metal, which, however, we do not see in Tucson. Apparently, V was scavenged by the early Sc-collecting phase (grossite, perovskite?) or by sulfides—much more so than Cr.

Origin of the Silicate Inclusions "Flow Pattern"

All small silicate inclusions in Tucson are about equi-dimensional, many of them even perfectly round (Figs. 2c and 2d). They are very similar in shape to chondritic constituents, in particular chondrules. In contrast to chondrules in chondrites, the two-phase droplets in Tucson are of a very simple construction: one or two olivine crystals immersed in glass. They seem to be the very primitive early condensation products of the solar nebula as predicted by the PLC model (e.g., Varela et al. 2005; Varela and Kurat 2009). They are rare in chondrites because constituents of chondrites commonly experienced continuous reaction with the cooling nebula gas and therefore evolved rather than remained witnesses of only the very early condensation process (e.g., Kurat 1988). Contemporaneous precipitation of metal and silicates at

the Tucson formation site provided ideal conditions for the preservation of the early condensation products (e.g., silicates) as they were immediately trapped and protected by the condensing metal. In this way, silicate inclusions survived almost unscarred in this meteorite and we get a glimpse at very early condensation processes in the solar nebula: liquid drops grow olivine crystals—physically similar but not identical to what happens in ice-growing water droplets uncountable times in our terrestrial atmosphere (e.g., Djikaev et al. 2002).

A large number of small silicate inclusions in Tucson were not trapped in time by metal. They thus were exposed to postformational alteration reactions with the solar nebula (Figs. 3a–f). Typically, they consist of a single olivine which was in part transformed into Al-rich pyroxene and brezinaite-Al-rich enstatite symplectites. What is seen in polished sections are either special cuts of larger silicate inclusions or these inclusions remained small because no aggregation partner was available before they got trapped in the metal. There are many indications (e.g., glass, very fine-grained metal) that only little time was available during formation of Tucson, thus both possibilities need to be taken into account.

All large silicate inclusions in Tucson are elongated (Figs. 1, 2a, 4a, and 4b) and consist of olivines and Al-poor enstatites glued together by Al-rich enstatite, mesostasis, or brezinaite-Al-rich enstatite symplectites. This particular shape apparently indicates ballistic aggregation, which requires aggregation partners to move in a single preferred direction (e.g., Sander 1986). The accretion structure of Tucson also contains portions which are reminiscent of the very common chondritic accretion structures, which typically are large (1–>10 cm) round balls (e.g., Skripnik 1988) and which are visible at large cut surfaces of Tucson (Fig. 1a).

Genetic Model for Tucson: A Proposal

From all of our observations and those of others we conclude that Tucson probably is a child of the solar nebula and a relative of chondrites. In particular, its silicate inclusions share many features with silicate-rich constituents of Renazzo (CR3)—as has already been recognized by Prinz et al. (1987). Tucson's silicate-rich objects differ from those of Renazzo by containing a record of extremely reducing conditions (very low FeO contents of silicates), high S fugacity (Cr, Ti, and Nb are predominately chalcophile), metal, and silicate precipitation as predicted by high-p condensation models, and unusual aggregate formation. Tucson carries evidence for coprecipitation of metal and silicates from the solar nebula gas. This situation allowed trapping of early silicates as well as of evolved silicate aggregates before volatile elements became oversaturated in the nebula. Consequently, Tucson silicates are among the objects poorest in volatile elements known from meteorites. Metal of Tucson is also highly deficient in the volatile elements Ga and Ge. The threshold temperature appears to be approximately 1000 K (for 10^{-4} bar): all elements with 50% condensation $T < 1060$ K (Au; Lodders 2003) are strongly depleted with respect to their cosmic abundances. In particular, Na (958 K), K (1006 K), Rb (800 K), Ga (968 K), and Ge (883 K) are almost nonexistent in Tucson.

Silicates and metal indicate formation at high temperature (~1800 K) and fast cooling. The latter resulted in the preservation of abundant glasses in the silicate inclusions and fine-grained duplex ataxite bulk metal (Buchwald 1975). Tucson obviously differs from chondrites by its very high metal content (~90 vol%), which is comparable to that of metal-rich CB chondrites (e.g., Newsom and Drake 1979; Grossman et al. 1988; Weisberg et al. 1990; Krot 2002). However, it differs from CB (and less metal-rich CH) chondrites by its lack of a breccia structure, BO chondrules and large BO and BOP objects. Tucson appears to be a meteoritic rock of its own with strong connections to primitive constituents of Renazzo and with some connection to enstatite meteorites as indicated by the presence of Al- and trace element-poor clinoenstatite.

Nehru et al. (1982) concluded that Tucson is a high-temperature (~1500 °C) impact mix of silicates and metal, which lost its volatile elements in that process. The assembly then rapidly cooled and thus preserved glasses and metastable Al-rich enstatite. However, there is no indication whatsoever for the action of shock and already Wänke et al. (1983) pointed out that an almost complete removal of alkalis and other volatile elements seems to be hard to achieve "on a fast time scale." They suggest that "The association of high reduction and depletion of elements with volatile character may relate Tucson to the metal phase of component A in the planet formation model of Wänke (1981)," i.e., a primitive matter.

CONCLUSIONS

Our chemical and petrological study of all phases present in the Tucson meteorite shows that the igneous model for the formation of the silicate inclusions needs to be revised. Glasses in the Tucson iron meteorite provide a set of data that strengthens the PLC model and provides arguments for an additional step toward meteorite unification. Beyond the element abundance data, the particular textures shown by silicate inclusions, in which olivines have crystal faces only in

contact with the glass, might serve as a natural example for the proposed growing mechanism of crystals from a vapor with the help of a liquid. Variation in the redox conditions, as indicated by the sulfide/silicate partition coefficient, governed the late formation stage of these inclusions when the metastable aluminous pyroxenes could have formed. All phases in Tucson, silicates and metal, appear to have a simple, one-step nebular origin after which they became isolated and protected from subsequent processing.

We propose that Tucson is a unique member of the primitive CR chondrite clan as defined by Weisberg et al. (1995) and Krot (2002).

Acknowledgments—We are grateful to Misha Nazarov (Moscow) for constructive discussions and to Theo Ntaflos (Vienna) for constant help with the EMP analysis. We are grateful for the thorough reviews by H. Palme and A. Ruzicka and by the careful handling of the associate editor E. Scott. Financial support was received from FWF, Austria (P16420-N10, P20226-N10), from CONICET (PIP 1645), Agencia (PICT212) and CONICET-FWF and CONICET-NSF International Cooperation Projects, Argentina, and NASA.

Editorial Handling—Dr. Edward Scott

REFERENCES

Anders E. and Grevesse N. 1989. Abundances of the elements: Meteoritic and solar. *Geochimica et Cosmochimica Acta* 53:197–214.

Balabin A. I., Osadchii E. G., Urusov V. S., and Senin V. G. 1986. Phase relations of participating daubreelite in systems of Fe-Cr-S, Mn-Fe-S, and Mg-Fe-Cr-S, at 840, 745, 660, and 550 C. *Geokhimiia* 1:35–48. In Russian.

Berg T., Marosits E., Maul J., Schönhense G., Hoppe P., Ott U., and Palme H. 2009. Evidence of nebular condensation of sub-microns refractory metal alloys (abstract #1585). 40th Lunar and Planetary Science Conference. CD-ROM.

Boesenberg J. S. and Ebel D. S. 2009. Experiments to confirm condensed phase assemblages predicted by equilibrium thermodynamic calculation in dust-enriched systems: Preliminary results (abstract #2125). 40th Lunar and Planetary Science Conference. CD-ROM.

Borisov A. and Palme H. 1995. The solubility of iridium in silicate melts: New data from experiments with $Ir_{10}Pt_{90}$ alloys. *Geochimica et Cosmochimica Acta* 59:481–485.

Buchwald V. 1975. *Handbook of iron meteorites*, vol. 3. Berkeley, California: University of California Press. 1418 p.

Bunch T. E. and Fuchs L. H. 1969. A new mineral: Brezinaite, Cr_3S_4 and the Tucson meteorite. *American Mineralogist* 54:1509–1518.

Campbell A. J. and Humayun M. 2004. Formation of metal in the CH chondrites ALH 85085 and PCA 91467. *Geochimica et Cosmochimica Acta* 68:3409–3422.

Chaussidon M., Libourel G., and Krot A. 2008. Oxygen isotopic constraints on the origin of magnesian chondrules and on the gaseous reservoirs in the early solar system. *Geochimica et Cosmochimica Acta* 72:1924–1938.

Chou C. L., Baedecker P. A., and Wasson J. T. 1973. Distribution of Ni, Ga, Ge and Ir between metal and silicate portions of H-group chondrites. *Geochimica et Cosmochimica Acta* 37:2159–2171.

Cohen E. 1905. *Meteoritenkunde*. Stuttgart, Band III: Schweizerbart'sche Verlagsbuchhandlung. pp. 88–100.

Djikaev Y. S., Tabazadeh A., Hamil P., and Reiss H. 2002. Thermodynamic conditions for the surface-stimulated crystallization of atmospheric droplets. *The Journal of Physical Chemistry, Series A* 106:10247–10253.

Ebel D. S. 2006. Condensation of rocky material in astrophysical environments. In *Meteorites and the early solar system II*, edited by Lauretta D. S. and McSween H. Y. Tucson, AZ: The University of Arizona Press. pp. 253–277.

Ebel D. and Grossman L. 2000. Condensation in dust-enriched systems. *Geochimica et Cosmochimica Acta* 64:339–366.

Engler A., Varela M. E., Kurat G., Ebel D., and Sylvester P. 2007. The origin of non-porphyritic pyroxene chondrules in UOCs: Liquid solar nebula condensates? *Icarus* 192:248–286.

Fegley B. and Palme H. 1985. Evidence for oxidizing conditions in the solar nebula from Mo and W depletions in refractory inclusions in carbonaceous chondrites. *Earth and Planetary Science Letters* 72:311–326.

Givargizov E. I. 1987. *Highly anisotropic crystals*. Dordrecht: D. Reidel. 394 p.

Green T. H. 1994. Experimental studies of trace-element partitioning applicable to igneous petrogenesis—Sedona 16 years later. *Chemical Geology* 117:1–36.

Grossman L. and Olsen E. 1974. Origin of the high temperature fraction of C2 chondrites. *Geochimica et Cosmochimica Acta* 38:173–187.

Grossman J. N., Rubin A. E., and MacPherson G. J. 1988. ALH 85085: A unique volatile-poor carbonaceous chondrite with possible implications for nebular fractionation processes. *Earth and Planetary Science Letters* 91:33–54.

Jones R. H., Leshin L., Guan Y., Sharp Z. D., Durakiewicz T., and Schilk A. J. 2004. Oxygen isotope heterogeneity in chondrules from theMokoiaCV3 carbonaceous chondrite. *Geochimica et Cosmochimica Acta* 68:3423–3438.

Kennedy A. K., Lofgren G. E., and Wassenburg G. J. 1993. An experimental study of trace element partitioning between olivine, orthopyroxene and melt in chondrules: Equilibrium values and kinetic effects. *Earth and Planetary Science Letters* 115:177–195.

Kobatake H., Tsukamoto K., Nozawa J., Nagashima K., Satoh H., and Dold P. 2008. Crystallization of cosmic dust from highly supersaturated silicate vapor in a rapidly cooled environment. *Icarus* 198:208–217.

Koblitz J. 2003. *Metbase*. CD-ROM. www.metbase.de/home.html.

Krot A. E. 2002. The CR chondrite clan: Implications for early solar system processes. *Meteoritics & Planetary Science* 37:1451–1490.

Kurat G. 1967. Einige Chondren aus dem Meteoriten von Mezö-Madaras. *Geochimica et Cosmochimica Acta* 31: 1843–1857.

Kurat G. 1988. Primitive meteorites: An attempt towards unification. *Philosophical Transactions of the Royal Society of London* 325:459–482.

Kurat G., Varela M. E., Hoppe P., and Clocchiatti R. 1997. Glass inclusions in Renazzo olivine: Condensates from the solar nebula? (abstract). *Meteoritics & Planetary Science* 32:A76.

Kurat G., Varela M. E., Zinner E., Maruoka T., and Brandstätter F. 2003. Major and trace elements in some glasses from the NWA 1664 howardite (abstract #1733). 34th Lunar and Planetary Science Conference. CD-ROM.

Kurat G., Zinner E., and Varela M. E. 2007. Trace element studies of silicate-rich inclusions in the Guin (UNGR) and Kodaikanal (IIE) iron meteorites. *Meteoritics & Planetary Science* 42:1441–1463.

Libourel G. 1999. Systematics of calcium partitioning between olivine and silicate melt: Implications for melt structure and calcium content of magmatic olivines. *Contributions to Mineralogy and Petrology* 136:63–80.

Libourel G., Krot A., and Tissandier L. 2006. Role of gas-melt interaction during chondrule formation. *Earth and Planetary Science Letters* 251:232–240.

Lodders K. 2003. Solar system abundances and condensation temperatures of the elements. *The Astrophysical Journal* 591:1220–1247.

Lodders K. and Fegley B. 1998. *The planetary scientist's companion*. New York: Oxford University Press. 371 p.

McKay G. A. and Weill D. F. 1977. KREEP petrogenesis revisited. Proceeding, 8th Lunar Science Conference. pp. 2339–2355.

Meibom A., Petaev M. I., Krot A. K., Wood J. A., and Keil K. 1999. Primitive FeNi metal grains in CH carbonaceous chondrites formed by condensation from a gas of solar composition. *Journal of Geophysical Research* 104:22,053–22,059.

Mitsui H., Oikawa K., Ohnuma I., Kainuma R., and Ishida K. 2002. Morphology of sulfide formed in the Fe-Cr-S ternary alloys. *ISIJ International* 42:1297–1302.

Miyake G. T. and Goldstein J. 1974. The Tucson meteorite. *Geochimica et Cosmochimica Acta* 38:1201–1212.

Nehru C. E., Prinz M., and Delaney J. S. 1982. The Tucson iron and its relationship to enstatite chondrites (abstract). Proceedings, 13th Lunar and Planetary Science Conference. *Journal of Geophysical Research* 87:A365–A373.

Newsom H. E. and Drake M. J. 1979. The origin of metal clasts in the Bencubbin meteoritic breccia. *Geochimica et Cosmochimica Acta* 43:689–707.

Pack A. and Palme H. 2003. Partitioning of Ca and Al between forsterite and silicate melt in dynamic systems with implications for the origin of Ca-Al-rich forsterites in primitive meteorites. *Meteoritics & Planetary Science* 38:1263–1281.

Prinz M., Weisberg M. K., Nehru C. E., and Delaney J. S. 1987. Bencubbin, Kakangari, Tucson and Renazzo: A speculative connection between some of their major components (abstract). 18th Lunar and Planetary Science Conference. pp. 800–801.

Rambaldi E. 1976. Trace element content of metals from L-group chondrites. *Earth and Planetary Science Letters* 31:224–238.

Rammensee W., Palme H., and Wänke H. 1983. Experimental investigation of metal-silicate partitioning of some lithophile elements (abstract). 14th Lunar and Planetary Science Conference. pp. 628–629.

Sander L. M. 1986. Fractal growth processes. *Nature* 322:789–793.

Skripnik A. Ya. 1988. Accretion structures—I: Their relicts in chondrites and chondrule formation model (abstract). 19th Lunar and Planetary Science Conference. pp. 1091–1092.

Smith J. L. 1855. A description of five new meteoritic irons. *American Journal of Science, 2nd Series* 19:322–343.

Taylor S. R. 1992. *Solar system evolution: A new perspective*. Cambridge, UK: Cambridge University Press. 307 p.

Toppani A., Libourel G., Robert F., and Ghanbaja J. 2006. Laboratory condensation of refractory dust in protosolar and circumstellar conditions. *Geochimica et Cosmochimica Acta* 70:5035–5060.

Varela M. E. 2008. Heating experiments on glass inclusions in Allende (CV3) olivines: Clues to the formation conditions of chondrules? *Geochimica et Cosmochimica Acta* 72:3170–3183.

Varela M. E. and Kurat G. 2006. An universal meteorite formation process (abstract). *Meteoritics & Planetary Science* 41:A180.

Varela M. E. and Kurat G. 2009. Glasses in meteorites and the Primary Liquid Condensation Model. *Mitteilungen der Österreichischen Mineralogischen Gesellschaft* 155:279–320.

Varela M. E., Kurat G., Clocchiatti R., and Schiano P. 1998. The ubiquitous presence of silica-rich glass inclusions in mafic minerals: Examples from Earth, Mars, Moon and the aubrite parent body. *Meteoritics & Planetary Science* 33:1041–1051.

Varela M. E., Kurat G., Hoppe P., and Brandstaetter F. 2002. Chemistry of glass inclusions in olivines of the CR chondrites Renazzo, Acfer 182, and El Djouf 001. *Geochimica et Cosmochimica Acta* 66:1663–1679.

Varela M. E., Kurat G., Zinner E., Métrich N., Brandstätter F., Ntaflos T., and Sylvester P. 2003. Glasses in the D'Orbigny angrite. *Geochimica et Cosmochimica Acta* 67:5027–5046.

Varela M. E., Kurat G., and Zinner E. 2005. A liquid-supported condensation of major minerals in the solar nebula: Evidence from glasses in the Kaba (CV3) chondrite. *Icarus* 178:553–569.

Varela M. E., Kurat G., and Zinner E. 2006. The primary liquid condensation model and the origin of barred olivine chondrules. *Icarus* 184:344–364.

Varela M. E., Zinner E., and Kurat G. 2008. Glasses in Tucson (IRUNGR): A SIMS study (abstract #1373). 39th Lunar and Planetary Science Conference. CD-ROM.

Varela M. E., Zinner E., and Kurat G. 2009. SIMS study of Tucson (IRUNGR) silicates (abstract #5091). *Meteoritics & Planetary Science* 44:A210.

Varela M. E., Kurat G., Zinner E., and Brandstätter F. 2010. The Tucson ungrouped iron meteorite: A step in deciphering its enigmatic origin (abstract #1316). 41st Lunar and Planetary Science Conference. CD-ROM.

Wai C. M. and Wasson J. 1969. Silicon concentration in the metal of the iron meteorites. *Geochimica et Cosmochimica Acta* 33:1465–1471.

Wänke H. 1981. Constitution of terrestrial planets. *Philosophical Transactions of the Royal Society of London* 303:287.

Wänke H., Dreibus G., Huth J., Huth H., Palme H., and Spettel B. 1983. Tucson anomalous iron meteorite: A special caprice of nature or more? (abstract). *Meteoritics* 18:416.

Wasson J. 1970. Ni, Ga, Ge and Ir in the metal of the iron-meteorites-with-silicate-inclusions. *Geochimica et Cosmochimica Acta* 34:957–964.

Weinbruch S., Palme H., and Spettel B. 2000. Refractory forsterite in primitive meteorites: Condensates from the solar nebular? *Meteoritics & Planetary Science* 35:161–171.

Weisberg M. K., Prinz M., and Nehru C. E. 1990. The Bencubbin chondrite breccia and ist relationship to CR chondrites and the ALH 85085 chondrite. *Meteoritics* 25:269–279.

Weisberg M. K., Prinz M., Clayton R. N., Mayeda T. K., Grady M. M., and Pillinger C. T. 1995. The CR chondrite clan. *Proceedings of the NIPR Symposium on Antarctic Meteorites* 8:11–32.

Yoneda S. and Grossman L. 1995. Condensation of CaO-MgO-Al_2O_3-SiO_2 liquids from cosmic gases. *Geochimica et Cosmochimica Acta* 59:3414–3444.

Zajacz Z. and Halter W. 2007. LA-ICPMS analyses of silicate melt inclusions in co-precipitated minerals: Quantification, data analysis and mineral/melt partitioning. *Geochimica et Cosmochimica Acta* 71:1021–1040.

Zinner E. and Crozaz G. 1986. A method for the quantitative measurement of rare earth elements in the ion microprobe. *International Journal of Mass Spectrometry and Ion Processes* 69:17–38.